12-9-2013

Using Delay-Differential Equations for Modeling Calcium Cycling in Cardiac Myocytes

Ryan Thompson

Using Delay-Differential Equations for Modeling Calcium Cycling in Cardiac Myocytes

by

Ryan Thompson

A thesis submitted in partial fulfillment of the
requirements for the degree of Master of Science
in Applied and Computational Mathematics
from the School of Mathematical Sciences
Rochester Institute of Technology

December 9, 2013

Signature of the Author Ryan Thompson

Accepted by Dr. Nathan Cahill 12/9/2013
Coordinator, M.S. Degree Program Date

SCHOOL OF MATHEMATICAL SCIENCES
ROCHESTER INSTITUTE OF TECHNOLOGY
ROCHESTER, NEW YORK

CERTIFICATE OF APPROVAL

M.S. DEGREE THESIS

The M.S. Degree Thesis of Ryan Thompson
has been examined and approved by the
thesis committee as satisfactory for the
thesis required for the M.S. degree
in Applied and Computational Mathematics

Dr. Elizabeth Cherry

Thesis Advisor

Dr. Tamas Wiandt

Thesis Committee

Dr. Niels Otani

Thesis Committee

12/9/2013

Date

THESIS RELEASE PERMISSION
ROCHESTER INSTITUTE OF TECHNOLOGY
SCHOOL OF MATHEMATICAL SCIENCES

Title of Thesis:

Using Delay-Differential Equations for Modeling Calcium Cycling in Cardiac Myocytes

I, Ryan Thompson, hereby grant permission to Wallace Memorial Library of R.I.T. to reproduce my thesis in whole or in part. Any reproduction will not be for commercial use or profit.

Signature Ryan Thompson 12/9/2013
Date

Using Delay-Differential Equations for Modeling Calcium Cycling in Cardiac Myocytes

by

Ryan Thompson

Submitted to the
School of Mathematical Sciences
in partial fulfillment of the requirements
for the Master of Science Degree
in Applied and Computational Mathematics
at the Rochester Institute of Technology

Abstract

The cycling of calcium at the intracellular level of cardiac cells plays a key role in the excitation-contraction process. The interplay between ionic currents, buffering agents, and calcium release from the sarcoplasmic reticulum (SR) is a complex system that has been shown experimentally to exhibit complex dynamics including period-2 states (alternans) and higher-order rhythms. Many of the calcium cycling activities involve the sensing, binding, or diffusion of calcium between intracellular compartments; these are physical processes that take time and typically are modeled by "relaxation" equations where the steady-state value and time course of a particular variable are specified through an ordinary differential equation (ODE) with a time constant. An alternative approach is to use delay-differential equations (DDEs), where the delays in the system correspond to non-instantaneous events. In this thesis, we present a thorough overview of results from calcium cycling experiments and proposed intracellular calcium cycling models, as well as the context of alternans and delay-differential equations in cardiac modeling. We utilize a DDE to model the diffusion of calcium through the SR by replacing the relaxation ODE typically used for this process. The relaxation time constant τ_a is replaced by a delay δ_j, which could also be interpreted as the refractoriness of ryanodine receptor channels after releasing calcium from the sarcoplasmic reticulum. This is the first application of delay-differential equations to modeling calcium cycling dynamics, and to modeling cardiac systems at the

cellular level. We analyzed the dynamical behaviors of the system and focus on the factors that have been shown to produce alternans and irregular dynamics in experiments and models with cardiac myocytes. We found that chaotic calcium dynamics could occur even for a more physiologically revelant SR calcium release slope than comparable ODE models. Increasing the SR release slope did not affect the calcium dynamics, but only shifted behavior down to lower values of the delay, allowing alternans, higher-order behavior, and chaos to occur for smaller delays than in simulations with a normal SR release slope. For moderate values of the delay, solely alternans and 1:1 steady-state behavior were observed. Above a particular threshold value for the delay, chaos appeared in the dynamics and further increasing the delay caused the system to destabilize under broader ranges of periods. We also compare our results with other models of intracellular calcium cycling and suggest promising avenues for further development of our preliminary work.

Acknowledgements

First off, I would like to thank Dr. Elizabeth Cherry for guiding me on this project and in being very meticulous with all aspects of the document. It has been a wonderful and challenging learning experience that I'm sure will prove to be priceless in the future. I'd also like to thank Dr. Tamas Wiandt for his help in getting my feet wet in delay-differential equations, and for helping me out with any problems I ran across in solving delay-differential equations. I also would like to thank Dr. Niels Otani for his valued advice and comments, even in the short time I have known him. I'd like to acknowledge family and friends, staff and colleagues, all of which have been extremely supportive throughout my years at the Rochester Institute of Technology. Finally, I'd like to thank the National Science Foundation for funding this project through NSF grant CMMI - 1028261.

Contents

List of Figures

Chapter 1

Introduction

Heart disease is one of the leading causes of death in the industrialized world. For the years 1999-2009, cardiovascular disease was responsible for 32.3% of all deaths in the United States, or about 1 out of every 3 deaths [23]. Some of these deaths are sudden and asymptomatic, making prediction of these dangerous cardiovascular events an extremely difficult task. Cardiovascular events such as an arrhythmia can occur when the rhythm of electrical signals within the cardiac tissue becomes disordered, resulting in an ineffective contraction of the heart. Arrhythmias such as ventricular tachycardia and fibrillation are life-threatening situations where conduction signals become uncoordinated in heart tissue. It is becoming widely accepted that life-threatening arrhythmias could originate from instabilities in the cardiac action potential [13, 33, 40].

A cardiac action potential is a physical event when the electrical membrane potential of a myocyte sharply jumps (depolarization), and then returns to a lower resting potential (repolarization), all within a time frame of hundreds of milliseconds. Action potentials are a major aspect of cell-to-cell communication and initiate intracellular processes (including calcium cycling activities) in excitable cells, such as muscle cells in the heart. Voltage-gated ionic channels regulate the electrical potential via the flow of ions across the cell's membrane. The concentration of calcium ions rises in the bulk myoplasm, and leads to the contraction process of the cell.

The processes within cardiac myocytes during the course of an action potential are relatively well-known, but the role of the membrane potential, intracellular calcium, and their coupling in the production of arrhythmias is not yet fully understood. Experiments in and mathematical models of cardiac myocytes have worked to provide better insight to the dynamics of cardiac behavior, with the goal of facilitating the development of anti-arrhythmic drugs and procedures that can be used in a clincal setting to reduce the risk of cardiac-related death and disease. Mathematical models have been used to describe cardioelectrophysiology at the subcellular level to the level of whole tissue, and continue to complement experiments performed in cardiac cells and tissue. These mathematical models have been proven to be helpful, as they can be used to test hypotheses that are otherwise impossible to resolve. As technology advances, new experimental methods and techniques allow scientists to observe more of the behavior within the complex cardiac system, and develop novel hypotheses for arrhythmogenesis.

In this thesis we suggest a novel approach to how the diffusion of calcium within a cardiac myocyte is modeled, specifically within the sarcoplasmic reticulum, an intracellular store of calcium. The standard for modeling this process is an ordinary differential equation, where the derivative depends on the difference between calcium concentrations in adjacent intracellular compartments and the rate at which diffusional steady-state is approached is determined by a time constant that is not readily known or experimentally observable. Our approach is to model this diffusion with a simple, first-order linear delay-differential equation, where the delay implemented represents the delay between calcium entering one compartment of the sarcoplasmic reticulum and diffusing into another part of the sarcoplasmic reticulum. We will adjust the delay, and analyze the dynamical consequences in the calcium cycling system proposed by Shiferaw et al in Ref. [49]. As far as we know, this is the first application of delay-differential equations to cardiac modeling at the cellular level and in modeling intracellular calcium cycling.

The remainder of this document is organized as follows. In Section 2 we present an overview of calcium cycling, and discuss the important features and phenomena of the intracellular calcium cycling system. In Section 3 we introduce the phenomenon of cardiac alternans and its implications. We also discuss possible mechanisms that could lead to alternans and review the results of literature on experiments and modeling approaches for alternans. In Section 4.1 we familiarize the reader with delay-differential equations

and outline some common applications of delay-differential equations to mathematical modeling. We describe our numerical method for solving a system of both ordinary and delay-differential equations in Section 4. We show the calcium cycling model that we are altering and discuss interpretations of replacing a time constant used in the original system with a delay. We also describe our method for determining calcium peaks in our simulations. Our results are examined in Section 5, where our model displays periodic behavior such as alternans as well as chaos. We also analyze the consequences of steepening the sarcoplasmic reticulum (SR) release slope, and develop approximate conditions for instability in our calcium cycling system of equations. We present our results and their implications in Section 6. Finally, we review some conclusions in Section 7 and suggest possible avenues for further development of our work.

Chapter 2

Overview of Calcium Cycling

In this section, we give an introduction to intracellular processes. Calcium plays an integral role in the excitation-contraction process of a cardiac cell by initiating the contraction of ventricular myocytes. Ventricular cardiac cells are of particular interest because they contract and pump blood, whereas other myocardial cells either do not contract or do so to a lesser degree. When a cardiac myocyte is depolarized during an action potential, intracellular protein kinases are activated. These proteins phosphorylate cellular proteins that open L-type calcium channels and allow calcium from extracellular spaces including T-tubules to flow into the cell. Phosphorylation of the L-type channels increases the influx of calcium ions into the myocyte. In close proximity to the L-type channels are ryanodine receptors (RyR), which, upon sensing an increase in local calcium concentration, release more calcium ions into the myoplasm from junctional sarcoplasmic reticulum (JSR) compartments. This release of calcium from JSR compartments is commonly called calcium-induced calcium release (abbreviated CICR), and during this process calcium ions are released into a subset of the bulk myoplasm called the submembrane space, which is modeled separately from the bulk myoplasm for convenience.

The influx of calcium into the submembrane space creates a steep diffusion gradient from the submembrane space to the bulk myoplasm. Some of these ions bind to buffers, such as troponin-C and calmodulin. Buffers are calcium-binding proteins that are responsible for cellular regulatory effects. There are also buffers within the sarcoplasmic reticulum (SR) such as calsequestrin, as well as in the SR membrane (phospholamban). The binding

of calcium ions to troponin-C in the myoplasm reduces the ability of troponin-1 to inhibit ATP-ases and leads to conformational changes in actin and myosin. The contraction of the cell occurs as myosin heads bind to actin filaments and flex. After the myocyte is signaled to contract by troponin-C, it must recover to prepare for the next action potential. The myocyte begins to relax as calcium ions are restored back into the SR. The protein phospholamban is responsible for regulating Ca^{2+} flow back into the sarcoplasmic reticulum. Once phospholamban is phosphorylated, sarcoendoplasmic reticulum calcium ATP-ase (SERCA) initiates the uptake of calcium from the bulk myoplasm into the SR. In addition, currents such as the Na^{+}-Ca^{2+} exchanger equilibrate calcium ion concentrations within and outside the cell, thereby restoring the cell to a relaxed, quiescent state. The calcium ions that were pumped into the SR via the uptake current then diffuse through the SR, which is sometimes modeled separately as the NSR (network sarcoplasmic reticulum) and JSR, completing the cycle. The NSR is a complex tubular network in which calcium ions flow to JSR compartments via diffusion (or out of JSR compartments, if the diffusion gradient is reversed) after being pumped back into the SR through uptake pumps. Two representations of the intracellular spaces and processes from different intracellular calcium cycling models are shown in Figure 2.1.

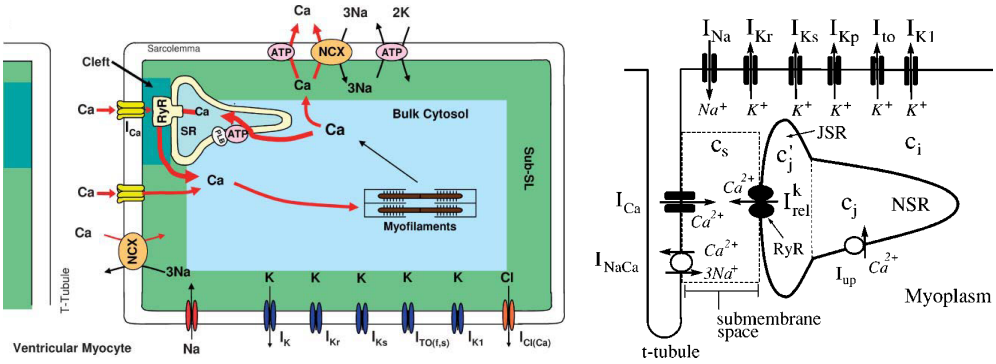

Figure 2.1: Diagrams of intracellular spaces in cardiac myocytes with the flow of calcium within the cell highlighted. Left: The cardiac cell is separated into four compartments: the SR, junctional cleft (also referred to as the submembrane space), the bulk cytosol (myoplasm), and the subsarcolemmal space (adjacent to the cell membrane, or sarcolemma). Calcium flows into the cell (I_{Ca}) through L-type calcium channels, which trigger the release of calcium from the SR after being sensed by ryanodine receptors (RyR). Calcium diffuses into the cytosol, where calcium binds to buffers such as troponin C (not shown), which in turn signals myofilaments to contract the cell. Exchanging currents such as the Na^+-Ca^{2+} return ionic species to diastolic (resting) levels. Diagram is from Ref. [48]. Right: The model cell is split up into four compartments as well: the myoplasm, submembrane space, and the SR is divided into the JSR and NSR. L-type calcium currents (I_{Ca}), SR release current (I^k_{rel}), uptake current (I_{up}), the Na^+-Ca^{2+} exchanger (I_{NaCa}), and other transmembrane currents are shown. Variables representing the calcium concentrations in different parts of the cell are displayed (e.g., c_i for the myoplasmic calcium concentration). Diagram is from Ref. [51].

Some of the earliest models of cardiac action potentials did not include calcium in their models; in particular, the first model was published at a time when calcium currents in cardiomyocytes had not yet been discovered [39]. Later attempts at modeling cardiac action potentials, sometimes referred to as second-generation models, incorporated phenomenological derivations of calcium cycling in their models that reproduced calcium uptake into the sarcoplasmic reticulum and release into the cytoplasm along with ion homeostasis - restoring pump and exchanger current, while the bulk intracellular calcium concentration displayed a time course similar to those observed by DiFrancesco et al. in experiments [17].

Beeler and Reuter developed a mathematical model describing the ventricular action potential, focusing on the role of the slow inward current. The slow inward current, mainly carried by calcium, was thought to play a significant role in the cardiac action potential and in the excitation-contraction process [3]. Beeler and Reuter and Luo et al. modeled the involvement of calcium phenomenologically within the formulation of the slow inward current, but they were not able to formulate a more sophisticated calcium cycling system since measurement of the intracellular calcium transient (myoplasmic calcium concentration during the course of an action potential) and SR calcium concentration were limited by the experimental technology available [3, 37].

Calcium cycling models are often built upon describing the individual processes physically and then determining how these parts of the calcium cycling system affect each other and the action potential. Some of the main features that calcium cycling models exhibit are calcium-induced calcium release and uptake into the SR via SERCA, as well as the role of the SR, L-type calcium channels and exchanging currents in the calcium cycling system. The remainder of this chapter describes intracellular calcium cycling in more detail.

2.1 Calcium-Induced Calcium Release

Calcium-induced calcium release (abbreviated CICR) is the process by which the release of calcium ions from the SR is triggered by an influx of calcium ions (through L-type calcium channels) that are in close proximity to ryanodine receptors which sense the increase in local calcium concentration. Eisner et al. proposed that the release of calcium from the SR depended on at least two things: the sensitivity of RyR channels to myoplasmic Ca^{2+} fluxes and the calcium content in the SR when a channel opens [18]. The release current formulated in Ref. [49] by Shiferaw et al. is proportional to the whole-cell L-type calcium current and incorporates a piece-wise-continuous release function dependent on the calcium content in the JSR compartments, which have the capability of fractional release. Lastly, a negative feedback mechanism is incorporated into the differential equation governing the release current. Within the release function, in conditions where the average JSR concentration is high, an adjustable constant represents the steepness of the dependence of the release current on the concentration of calcium in the JSR. Hund and Rudy's release current included an additional inactivation time constant that depended on calmodulin

protein kinase II (CaMKII) activity [31].

Ryanodine receptor channels are responsible for sensing changes of calcium concentrations in the myoplasm (predominantly in the subspace region near T-tubules) and consequently releasing calcium from the SR via CICR, which makes RyR a significant part of the intracellular calcium cycle. It is generally accepted that the open probability of release channels regulated by ryanodine receptors is affected by the calcium concentrations in the JSR compartments and in the defined subspace in close proximity to release channels and L-type calcium currents. Although it is thought that activation of RyR is by SR calcium content and that inactivation is regulated by cytosolic calcium, Hund and Rudy included CaMKII phosphorylation as an additional factor to promote opening of RyR channels [31]. The degree to which these influences actually determine the open probability of the RyR channels is not clear, as is evident in the literature. It is thought that the actual number of activated channels during systole is very small; peak open probabilities range from as low as 1% [48], up to 5% [38].

L-type currents are a key component of these models, as they are responsible for triggering the release of calcium from the sarcoplasmic reticulum sensed by RyR. Two main formulations of L-type current channels are used: either a Hodgkin-Huxley [29] approach with activation and inactivation gates or a Markovian approach [12] with multiple transitions between open and closed states of the channel. Previous modeling attempts [11, 20, 36] were common-pool models, that described the release currents as an averaged overall release from all channels. This has been shown to be inaccurate, as it does not always produce graded release. Shiferaw et al. implemented a formulation that sums up several thousand localized discrete events to produce an overall resulting current that produced graded release [49]. Graded release is a characteristic of intracellular calcium cycling where the magnitude of the release current from the SR is proportional to the L-type calcium current that triggered it. This is done through spark recruitment, where sparks trigger the release of calcium from the SR. A (calcium) spark is a localized release of calcium into the dyadic junction, an intracellular area between L-type channels and ryanodine receptors. A recruited spark is a local release calcium that is sensed by RyR, and triggers that RyR release channel to open. As calcium is released into the localized area from RyR channels, the increase in calcium triggers neighboring RyR channels to release calcium from the SR as well. This process of triggering nearby RyR can propagate

and are often called calcium waves as they travel along the SR. A Markovian approach was utilized by Mahajan et al. in formulating the L-type calcium channel [38]. Inactivation (closing of ionic gates that ceases the influx of calcium ions) of the L-type channel was modeled to occur in two ways, through voltage-dependent inactivation and calcium-dependent inactivation. A main distinction between these two mechanisms is whether calcium is binding to calmodulin molecules to alleviate inhibition of inactivation or not.

2.2 Sarcoplasmic Reticulum

The sarcoplasmic reticulum (SR) stores calcium and, in conjunction with RyR, is responsible for the release of calcium into the myoplasm. As the concentration of calcium in the myoplasm rises, calcium binds with proteins that trigger contraction of the myocyte. The amount of calcium within the SR plays a critical role in how the cardiac myocyte behaves during an action potential. An important influence on SR calcium content is the calcium concentration in the bulk myoplasm. Simply put, the overall concentration of calcium in the bulk myoplasm is determined by the difference between the influx of calcium into the cell myoplasm through L-type and SR release currents, and efflux via exchanging currents and uptake pumps. A larger amount of calcium in the myoplasm will be sensed by SERCA uptake pumps, which then pump more calcium into the SR in order to fill JSR compartments so that Ca^{2+} is available for release during subsequent action potentials. SR calcium content also is dependent on the uptake pumps regulated by SERCA. A difference in the phosphorylation of SERCA could show differences in the SR calcium content within different levels of ventricular tissue, as experiments by Laurita et al. have shown [34]. Another modeling consideration is whether to model the SR as a single compartment [18, 37, 48], or to split the SR into the network SR (NSR) and the junctional SR (JSR) [17, 36, 38, 49]. Accounting for the separation of the NSR and JSR allows for the fact that calcium that is pumped into the SR through the uptake current is not immediately available, and must diffuse through the NSR to the JSR compartments in order to be available for release from the SR. The rate at which calcium flows through the SR is a detail that still requires further investigation, as we will discuss later in Section 4.3.

In addition to SR calcium content, the dependence of SR release on SR load can significantly affect the behavior of the calcium cycling model. The formula used in Ref. [18] by Eisner et al. was a simple Hill-type function, where the steepness of the relation could be altered by changing the value of the exponent to show a stronger relationship between SR calcium content and efflux from the SR. When this dependence becomes steep, chaos can occur in the system for rapid pacing, as shown by Shiferaw et al. [49] Eisner et al. found that an increase of SR calcium content led to a stronger efflux from the SR, resulting in a weaker influx from L-type currents [18]. Eisner at al. also determined that a steep relationship between SR calcium concentration and the amount of calcium released from the SR during an action potential can increase the fraction of SR content that is released [18].

2.3 SERCA Pump

After calcium is released from the SR into the bulk myoplasm, ions are pumped back into the SR via an uptake pump regulated by sarcoendoplasmic reticulum calcium ATP-ase (SERCA). Once the calcium is pumped back into the SR, it later refills the JSR compartments once the calcium ions have diffused through the NSR, so that the SR can properly release calcium upon the next stimulation. The SR uptake pump generally is modeled using a Hill function with exponent 2 [11, 38, 49], although others have included SR leak and backflux into their formulations of the uptake current [38, 47]. How the expression of SERCA varied throughout ventricular tissue was studied by Laurita et al. using experimental optical mapping techniques [34]. It was found that there was a transmural (depth-wise) heterogeneity in the behavior of cardiac tissue. At different levels of the tissue ranging from epicardial tissue near the surface of the heart down to endocardial tissue that lines the chambers of the heart, the recovery and duration of the calcium transient was significantly different. Laurita et al. defined the duration of the calcium transient as the difference in time from the onset of the calcium transient (20% above diastolic calcium levels), to resting of the calcium transient (when the intracellular level of calcium returns to within 90% of resting, diastolic levels) [34]. The connection between the larger transient duration, longer recovery time and the stronger presence of arrhythmias was attributed to a much lower expression of SERCA in endocardial tissue than in the epicardium.

2.4 Na^+-Ca^{2+} Exchanger

Following the triggered release from JSR compartments, calcium ions diffuse into the bulk myoplasm, where some of these ions bind to troponin C and initiate the contraction of the cardiac myocyte. Recovery of the cell is achieved partly through uptake currents into the NSR. But it also is necessary to extrude calcium that was brought into the cell via L-type currents, which is done by the Na^+-Ca^{2+} exchanger. This restores calcium concentrations within and outside the myocyte, but as a result, sodium ions begin to accumulate in the cell. To correct this, another exchanging current pumps sodium out of the cell, and draws potassium ions back into the cell. There are many transmembrane currents that are involved in maintaining ion homeostasis within the cardiac cell, and among the major currents are the SERCA uptake pump, the Na^+-Ca^{2+} exchanger and the Na^+-K^+ pump. When homeostasis is disturbed, the intracellular sodium concentration can accumulate, forcing the Na^+-Ca^{2+} exchanger to work harder, which results in a higher calcium content in the myoplasm during rapid pacing [27]. In the study of transmural heterogeneities by Laurita et al. [34], the activity of exchanging currents like the Na^+-Ca^{2+} exchanger was evaluated. It was determined that the Na^+-Ca^{2+} exchanger operated nearly identically throughout the tissue. The stronger tendency for endocardial tissue to be arrhythmogenic may be explained in part by the nonuniform activity of SERCA combined with a transmurally homogeneous behavior of the Na^+-Ca^{2+} exchanger, which could create disruptions in the intracellular homeostasis of ionic species.

2.5 Variations on Intracellular Calcium Cycling

There are physiological differences between ventricular myocytes in distinct species. Beyond that, there is a specialized fiber network in the heart that conducts electrical pulses faster than in other myocytes, with the purpose of ensuring synchronized contraction of the ventricles. This network is called the Purkinje network, and it is composed of Purkinje fibers that lie mainly within the endocardium in some species (such as canine and humans; an example cell is shown in Figure 2.2) but traverse the thickness of the heart wall in other species (pig, sheep) [2].

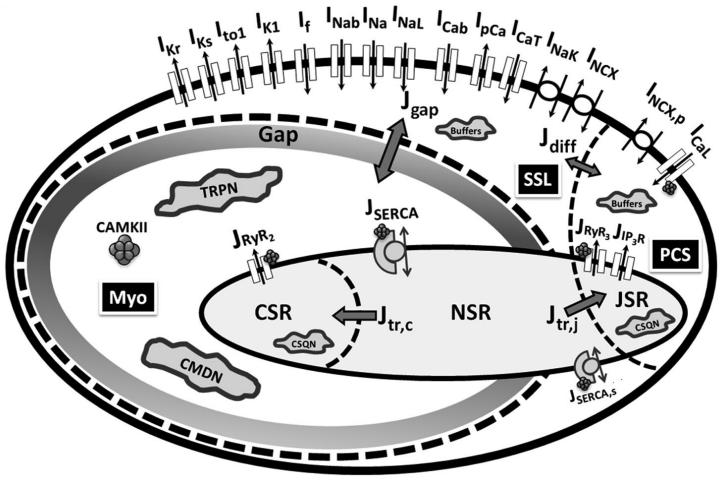

Figure 2.2: Schematic of a cardiac Purkinje cell from Ref. [35]. The model contains the following compartments: peripheral coupling subspace (PCS), subsarcolemma (SSL), bulk myoplasm (Myo), sarcoplasmic reticulum (SR), junctional SR (JSR), network SR (NSR), and corbular SR (CSR).

There are two major structural changes in the calcium cycling system in Purkinje cells compared to ventricular myocytes: an additional compartment within the SR, called the corbular SR (CSR), and the lack of T-tubular structure found in ventricle myocytes. The CSR, as opposed to the JSR, lies further inside the Purkinje cell, while JSR compartments are in close proximity to transmembrane currents such as the L-type calcium current. The lack of T-tubules and compartmentalization of ryanodine receptors RyR2, RyR3, and IP_3R (inositol triphosphate receptor) contribute to spatial heterogeneity of calcium cycling in Purkinje cells. Since the CSR is further away from the cell membrane where the PCS and SSL compartments are located, the CSR senses changes in only the bulk myoplasm calcium concentration [35]. In addition to these physical differences, there are additional discrepancies between Purkinje fibers and ventricular tissue in excitation-contraction process, such as buffering agents, since Purkinje fibers do not contract.

Chapter 3

Overview of Alternans

Alternans is a specific type of arrhythmia where the action potential duration (APD) alternates between long and short, in a period-2 behavior. Alternating behavior in the cardiac action potential has been observed in several abnormal circumstances, such as tachycardia. These observations suggest that alternans could be a predecessor to disorganized behavior in the heart.

The flow of ions across the myocyte membrane through voltage-gated ionic channels provide the increase in electrical potential that initiates an action potential. An action potential can also be started by a direct electrical stimulus, or the action potential of a neighboring cell can provide enough depolarizing current to reach threshold potential. Activation gates promote opening of ionic channels, while inactivation gates work as inhibitors to close ionic channels. Models that follow the Hodgkin-Huxley formalism [29] structure gating kinetics in the following way: the value of ionic gates ranges between zero (not permeable to ions) and one (fully permeable to ions). For a given type of ion channel, the product of the ionic gates resembles the percentage of conducting channels that are allowing ions to travel across the membrane. The gating variables are dependent on the membrane voltage, and also change in accordance with time constants associated with inactivation and activation of their respective ionic currents. Figure 3.1 plots an action potential, and the ionic gates and currents (including intracellular calcium), generated from the model presented in Ref. [37]. Once the myocyte is stimulated by an action potential, the fast sodium current allows Na^+ ions to rapidly flow into the cell, further increasing

the electrical potential and causing the spike in the cell membrane voltage. Note that the current contribution of I_{Na} peaks in magnitude at about -400 μA (the graph is truncated to show the other currents more clearly; note that inward currents have negative values by convention). The fast sodium current is active for only a few milliseconds and remains inactivated for the remainder of the action potential. With the sodium channels inactivated, sodium ions are actively transported out of the cell and potassium and calcium channels are activated, generating an outward flow of K^+ ions. As the calcium currents subside, the potassium currents repolarize the cell, returning it to its resting state in preparation for the next action potential.

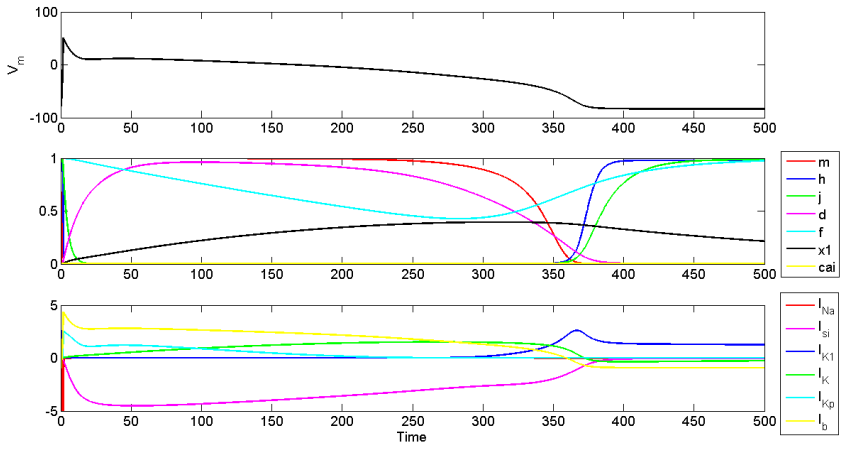

Figure 3.1: Top: A ventricular action potential for a single cell. Middle: Time course for ionic gates involved in the mathematical system of differential equations that comprise the ionic currents. m is an activation gate, and h and j are the fast and slow inactivation gates for the fast sodium current. d and f are the activation and inactivation gates for the slow inward current, respectively. $x1$ is an ionic gate for the time-dependent potassium current, and csi is the intracellular calcium concentration (on a much smaller scale than the ionic gates). Bottom: Ionic currents involved in the cardiac action potential. The currents shown are the fast sodium current (I_{Na}), slow inward current (I_{si}), a time-dependent and time-independent potassium current (I_K and I_{K1}), a plateau potassium current (I_{K_p}), and a background current (I_b). Adapted from Ref. [37].

The action potential duration (APD) is the time elapsed between depolarization (spike in voltage), and repolarization, when the voltage returns to resting (diastolic) levels. The

end of the APD is commonly 90% repolarization, when the membrane voltage returns to within 90% of resting potential (See Figure 3.2). The diastolic interval (DI) is the period of time that the membrane voltage is at resting, or diastolic levels. In other words, the DI is measured as the time from the end of the APD to the initiation of the succeeding action potential. Lastly, the cycle length (CL, also referred to as the period, T), is the sum of the APD and DI.

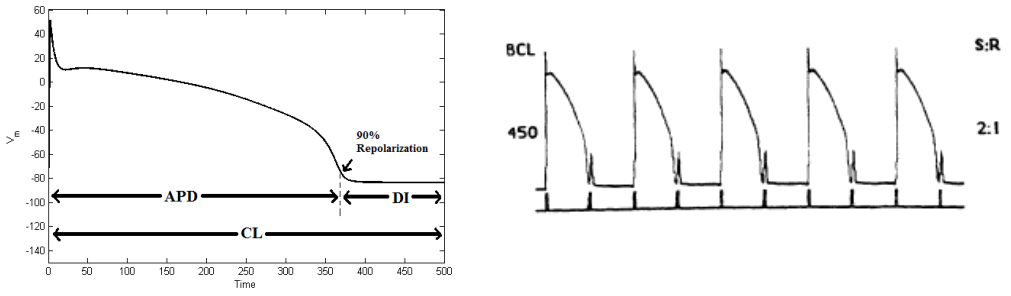

Figure 3.2: Left: Action potential with action potential duration (APD), diastolic interval (DI), and cycle length (CL) shown. Right: Action potentials at a basic cycle length (BCL) of 450 ms, exhibiting 2:1 conduction block. S:R is the stimulus-to-response ratio. Timing of the stimuli is marked below the action potentials. Every other stimulus fails to initiate an action potential, and the membrane voltage immediately returns to resting potential without producing an action potential. The right figure is from Ref. [37].

Alternans that is primarily driven by instabilities in the electrical potential is considered to be voltage-driven alternans and is evident by variances in the APD (see Figure 3.3). In cases where the tissue is paced rapidly, electrical waves can break up, producing an unstable state similar to fibrillation. Erratic changes in the dynamics of calcium in cardiac tissue also can promote alternans. An instability in intracellular calcium can cause disturbances in the APD, and the calcium transient is signficantly dependent on the action potential as well, so that calcium and voltage are bidirectionally coupled. In their experiments, Chudin et al. concluded that calcium instabilities could be the major factor in destabilizing ventricular tachycardia into fibrillation by altering the restitution properties of the APD [11]. Goldhaber et al. agreed with these findings but also stated that APD restitution slopes were not universally reliable at predicting the onset of alternans, and that the most likely explanation is that intracellular calcium dynamics plays a vital part in the genesis of alternans [24].

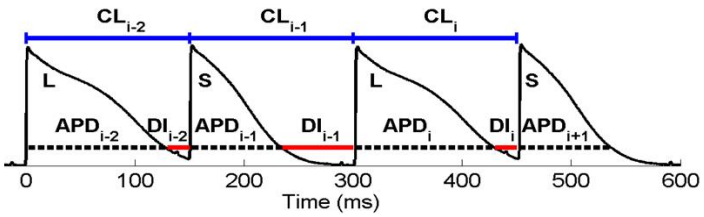

Figure 3.3: Voltage-driven alternans is displayed (alternating long and short APD). The cycle length (CL) was constant at 150 ms, and the amplitude of alternans appears to be about 50 ms (difference between APD_{i+1} and APD_i, or APD_{i-1} and APD_{i-2}). Figure is from Ref. [10].

3.1 APD Restitution

Nolasco and Dahlen devised a graphical method to study cardiac electrical alternans, with the goal of revealing arrhythmogenic conditions by making an analogy between the autoregulatory nature of cardiac tissue and an electrical feedback system [40]. By developing a transfer function relating each action potential to the previous diastolic interval, a diagram not unlike a cobweb diagram was used to show how the APD and DI evolved over iterations, and illustrate situations where alternans could arise. The postulates posed in this paper paved the way for future studies to investigate, confirm and/or refute conditions for cardiac alternans. Among the postulates is a decidedly controversial condition for alternans: the APD restitution curve slope criterion. Many studies and experiments have supported the claim that under conditions where the APD restitution curve's slope is above 1, unstable behavior can occur, including alternans [20, 21, 33, 45, 46, 53]. More recently, some studies have dissented from this, citing examples of alternans despite an APD restitution curve slope below 1 [11, 16, 24] and the role of calcium cycling in arrhythmogenesis [4, 11, 16, 24, 34, 43].

In addition to the slope of the APD restitution curve, the shape of the curve can have a dramatic effect on the dynamical behavior of the system. For example, Qu et al. determined in a modified Beeler-Reuter model that chaos only occurred for a nonmonotonic restitution curve when dealing with a one-dimensional ring of excitable tissue [45]. A monotonic APD restitution curve presented only quasiperiodic behavior followed by conduction block as the circumference decreased. On the other hand, the nonmonotonic

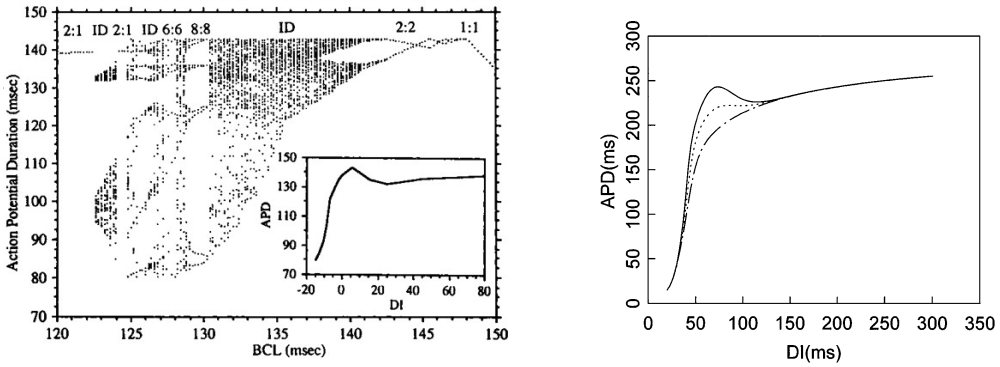

Figure 3.4: Left: Bifurcation diagram generated from iteration of the restitution function shown in the inset. Stable periodic patterns, irregular dynamics (chaos), and higher-order rhythms are indicated above the data points. From Ref. [52]. Right: The restitution curve becomes biphasic as a proportionality constant related to the maximum action potential duration increases, from Ref. [45].

(sometimes called biphasic) restitution curve showed quasiperiodic behavior, followed by a region of spatiotemporal chaos, and then eventually conduction block with decreasing circumference. Experiments by Watanabe et al. also showed that a nonmonotonic APD restitution curve could lead to complex dynamical behavior [52]. In Figure 3.4, a period-doubling cascade leads to chaos, but then a period-doubling reversal (also called period-halving cascade) happens in the shallow part of the curve after the critical point, returning to stable behavior.

3.2 Iterated Map Analysis

A commonly used method to model the nonlinear dynamics is to create a linear, one-dimensional discrete map that relates the APD of 2 neighboring beats via a restitution curve [40, 44, 49, 51]. A one-dimensional iterative map of SR calcium concentration was developed by Eisner et al. to study calcium alternans [18]. An example of this simple iterative map is shown in Figure 3.5. In light of conflicting evidence pertaining to the APD restitution slope criterion for alternans it has been suggested that low-dimensional stability analyses, although mechanistically insightful, may overlook more complex behaviors and systemic interactions. Motivated by this, Shiferaw et al. developed a 3-variable iterated

map to more fully encapsulate the coupled dynamics between voltage and calcium [51]. The 3 variables involve the APD, the bulk myoplasm Ca^{2+} concentration, and the Ca^{2+} concentration in the SR. This is done after collapsing the submembrane Ca^{2+} into the bulk myoplasm concentration and the JSR Ca^{2+} into the SR concentration, under the assumption that these pairs of concentrations are equilibrated in time for the next stimulus. Qu et al. developed a 3-variable iterated map to analyze stability of the calcium cycling system but utilized different variables than in Shiferaw et al. in Ref. [51], instead using equations for SR calcium release, SR calcium uptake, and APD restitution. Shiferaw et al. also have utilized a two-dimensional iterative map of the bidirectional coupling between calcium and voltage to study calcium and APD alternans [50].

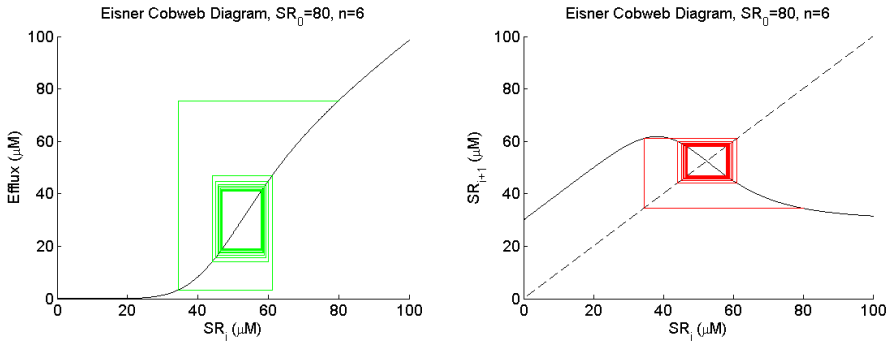

Figure 3.5: Cobweb diagrams displaying a periodic solution (period-2, alternans) for $n = 6, SR_0 = 80\ \mu M$. The iterative relations are $efflux = \frac{SR_i \times SR_i^n}{(K_d + SR_i^n)}$, and $SR_{i+1} = SR_i + influx - efflux$. The influx was assumed to be constant ($30\ \mu\ M$), as in Ref. [18]. Reproduced from [18].

3.3 SR Release Slope and Fractional Release

As discussed above, the SR content can have a significant effect on the magnitude of calcium release from the SR because of the steepness of the SR calcium release function. Eisner et al. mention in Ref. [18] that alternans could involve changes in the fraction of calcium released from the SR. Shannon et al. investigated fractional release in rabbit ventricular myocytes by isolating the SR release currents and SERCA uptake pumps through inhibition of the Na^+-Ca^{2+} exchanger [47]. In the experiments, it was shown that both

the free SR calcium concentration (calcium ions available for release from the SR) and the total SR concentration have a positive nonlinear relationship with the gain and fraction of calcium released from the SR. The gain of calcium released from the SR was measured as the total calcium released divided by the total trigger calcium (L-type calcium current). There were several trials where the fractional release was above 100%, explained by the re-release of calcium after it had been pumped back into the SR early in the action potential. It also was noted that even though the fractional release was above 100%, the SR never fully depleted during the course of SR calcium release (see Figure 3.6).

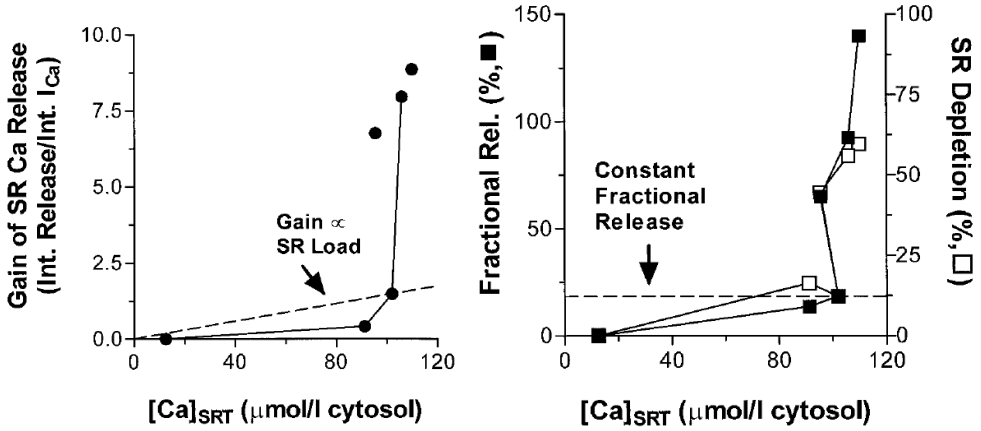

Figure 3.6: Steep nonlinear relationship between gain of SR release and fractional release with total SR calcium concentration. The slope becomes very steep at a SR concentration of $100\mu M$. Lowest levels of calcium in the SR were about 67% depleted. SR calcium content was extrapolated from the relationship between the total SR calcium concentration and pulse number measured by Shannon et al. Figures are from Ref. [47].

In Shiferaw's model of calcium cycling [49], the steepness of the SR release slope dramatically affected the dynamical behavior of the system. Alternans behavior was exhibited for rapid periodic pacing, but an increase in the release slope for high SR calcium concentrations allowed for chaotic behavior through a period-doubling bifurcation, displayed in Figure 3.8. Eisner et al. posed that alternans could happen in the following manner, given a steep relationship between SR calcium content and efflux. Figure 3.7 shows how the steepness of the dependence of SR content on SR calcium release can produce alternans. First the cell begins with a large SR calcium content, which results in a greater release of calcium from the SR via CICR. Then the next beat releases calcium from a

depleted SR, the result being a smaller efflux and thus a smaller calcium transient for that beat, leading to a net gain of calcium content in the SR for the following beat.

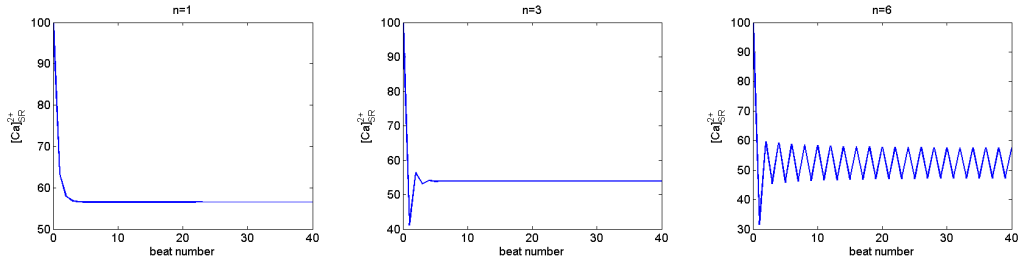

Figure 3.7: SR calcium content simulations for 40 beats, with increasing steepness (n) of SR release dependence on SR content. Stable alternans behavior occurs for $n = 6$. Note that the influx of calcium per beat was assumed to be constant. Adapted from Ref. [18].

Bien et al. studied cardiac alternans with a focus on quantifying the relationship between SR calcium content and calcium release from the SR under alternans conditions [4]. They concluded that a large SR content could lead to alternans in a similar way as suggested by Eisner et al. [18], and gave more precise details in the following process: first, a large SR content results in a large fractional release of calcium from the SR. This strong calcium release is well above a threshold value to produce calcium waves that propagate throughout the cell. Under a rapid pacing protocol, there is not enough time to restore calcium to the SR, and so the next stimulus produces a small calcium transient that does not reach the threshold value necessary to produce intracellular calcium waves. This alternation of small and large transient amplitudes can develop into alternans.

3.4 Transmural Heterogeneities

Many electrophysiological properties of ventricular myocytes, including ion channel functions and density, have been shown to vary with depth within the heart wall. Laurita et al. ([34]) studied how calcium is handled in different parts of ventricular tissue. They were able to reveal significant differences in how calcium affects ventricular tissue and showed a transmural (depth-wise) heterogeneity in the physiological response of endocardial, mid-myocardial, and epicardial tissues, presented in Figure 3.9.

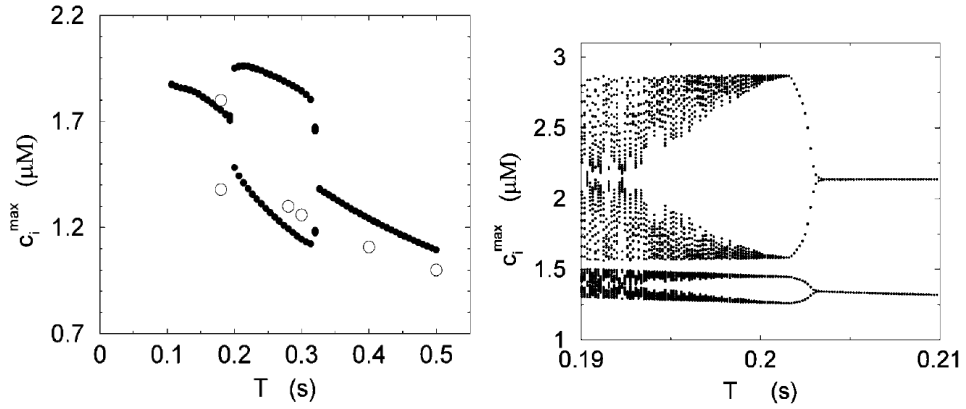

Figure 3.8: Left: Alternans behavior of peak myoplasmic calcium, with a SR release slope of 11.3 $\mu M/s$. Right: Period-doubling cascade leading to chaos, with a steeper release slope of 43.3 $\mu M/s$. Both graphs were produced by Shiferaw et al. in their intracellular calcium cycling model presented in Ref. [49]. Note that no chaotic behavior was observed for shallower SR release slopes.

Using optical mapping techniques, they were able to measure calcium transients and action potentials in their experiments quantitatively. Two of the main quantities compared throughout the tissue were τ, the relaxation time (also referred to as decay time) of the calcium transient, and CaF_{90}, the duration of the calcium transient (where F refers to the fluorescence signal being measured). Laurita et al. quantified calcium recovery through CaF_{90}, defined from 20% above the minimum diastolic value to when calcium returns to within 90% resting levels. They observed that the decay time τ was larger and CaF_{90} was longer in endocardial tissue than in the midmyocardial or epicardial tissue, meaning endocardial tissue recovered much more slowly than midmyocardial and epicardial tissue. Alternans was studied in the specimens via a rapid pacing protocol, and even though alternans did manifest in both endocardial and epicardial tissue simultaneously, alternating amplitudes were much more pronounced in the endocardium than in the epicardium. It was found that the change in the calcium transient amplitude in consecutive beats was 85% in endocardial tissue, which resembled alternans more distinctly than in the epicardium, which had a smaller difference of 15% in amplitude from beat to beat. In addition, endocardial tissue maintained a longer τ during alternans than epicardial tissue, but the action potential duration (APD) was consistently slightly longer in the epicardium than

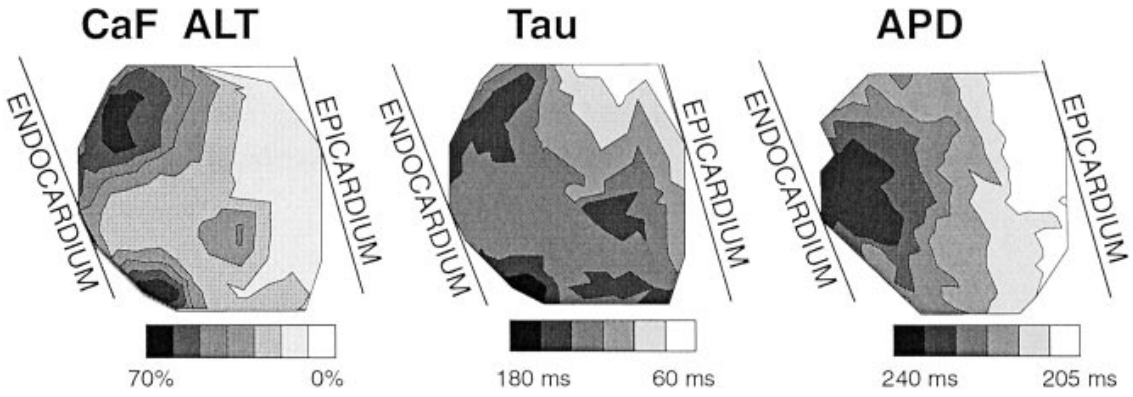

Figure 3.9: Contour maps measuring the degree of amplitude of alternans (CaF ALT), decay time of the calcium transient (Tau), and action potential duration (APD) from experiments in Ref. [34]. CaF ALT and Tau show similar patterns throughout the tissue, while the pattern of APD through the tissue was significantly different.

in endocardial tissue. Interestingly, APD restitution did not vary throughout the tissue, and the restitution curve slopes for both the endocardium and epicardium were well below 1 even despite the occurrence of alternans.

3.5 Voltage-Calcium Coupling

The intracellular calcium cycling system exhibits a codepedence of voltage and calcium, which comes from the influence of intracellular calcium on the membrane currents and the effect of the action potential on the calcium transient. A large release from the SR produces a large calcium transient, which works to inactivate the L-type calcium currents. The quicker the inactivation, the shorter the APD is. This, in turn increases the force with which the Na^+-Ca^{2+} exchanger extrudes calcium from the cell. The exchanger lengthens the APD due to the inward membrane current it generates. So, the amount with which the L-type currents and the Na^+-Ca^{2+} are involved during the action potential can have a lengthening or shortening effect on the duration of the action potential. The coupling between voltage and calcium is controlled by an exponent in the definition of the inactivation gate of the L-type calcium current in Refs. [44, 51]. A positive coupling causes the L-type calcium current to inactivate more slowly, allowing the SR to release more calcium. This

results in a larger calcium transient, which prolongs the APD. On the other hand, a negative coupling does the opposite: the L-type current is inactivated more quickly, providing a smaller SR release and calcium transient, which brings about a shorter APD. A simple diagram depicting these effects is shown in Figure 3.10. Note that positive and negative voltage-calcium coupling does not directly correspond to electromechanically concordant or discordant alternans, discussed in Sections 3.6 and 3.7. The coupling between voltage and calcium simply determines how the L-type calcium current works to extend the duration of the action potential, or hastens inactivation of the SR calcium current after SR calcium release, and consequently shortens the APD.

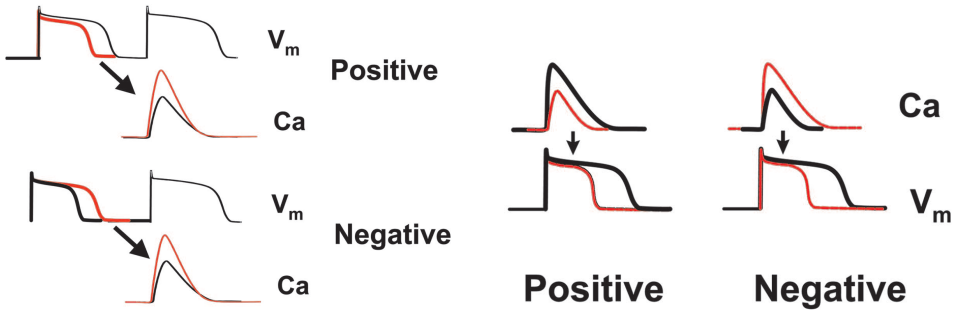

Figure 3.10: An illustration of bidirectional coupling between calcium and voltage from Ref. [50]. Left: Examples of positive and negative coupling between the APD and the following calcium transient on the next beat. Right: Examples of positive and negative coupling between the calcium transient and the APD on the same beat.

3.6 Electromechanically Concordant Alternans

Electromechanically concordant alternans (CA) occurs when alternating action potential durations coincide with the magnitude of the calcium transient (as opposed to spatially concordant alternans). In other words, a long APD corresponds to a large calcium transient, which is followed by a short APD and small calcium transient on the subsequent beat. In Shiferaw et al., the route to dynamical instability was always through a period-doubling bifurcation when voltage and calcium were positively coupled, and solely developed electromechanically concordant alternans [51]. Concordant alternans occurred in this situation regardless of whether voltage or calcium was the major instability mechanism at work (see

Figure 3.11). In Qu et al., concordant alternans manifested under several different conditions with both positive and negative couplings [44]. For a negative coupling between calcium and voltage, concordant alternans only occurred when the steepness of the SR release function was the sole major factor in causing dynamical instability, as Figure 3.14 shows.

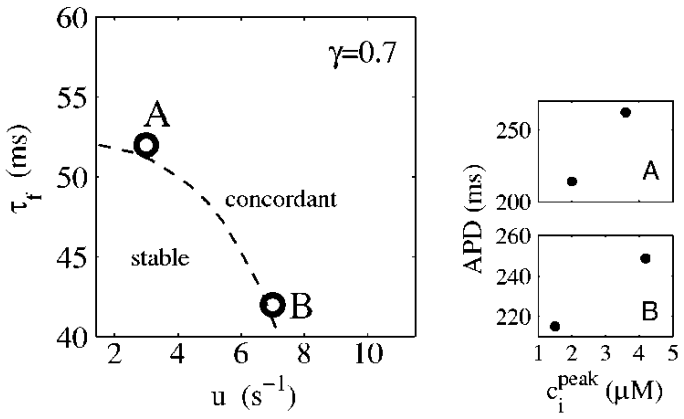

Figure 3.11: Stability boundaries for positive voltage-calcium coupling (exponent < 1, $\gamma = 0.7$ in Ref. [51]). τ_f is the time constant associated with inactivation of the L-type current, and u determines the steepness of SR release. Stable 1:1 (stimulus to response) rhythms are observed for small values of both τ_f and u. Consistent concordant alternans behavior occurs along the dotted line in the figure. High-order rhythms and chaos are observed further out from the boundary. Examples of the dynamics near the boundary are given to the right by plots of peak calcium concentration versus APD. Figure are from Ref. [51].

Concordant alternans also is possible when voltage and calcium are negatively coupled as the time constant of the L-type calcium current is increased. The L-type current lasts longer during an action potential, which steepens APD restitution. Consequently voltage dominates over calcium, and instability occurs via a period-doubling cascade to chaos, mainly caused by a steep APD restitution curve slope [51].

3.7 Electromechanically Discordant Alternans

Electromechanically discordant alternans (DA), as opposed to concordant alternans, is when the APD and calcium transient are offset, when a long APD produces a small calcium transient, and the next beat produces a short APD but a large calcium transient. An example is shown in Figure 3.12, where the APD and the calcium transient alternate.

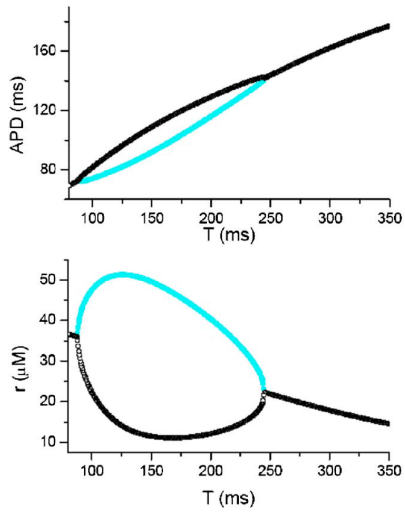

Figure 3.12: Bifurcation diagram for negative voltage-calcium coupling (below 0 in Ref. [44]). Above, APD is plotted versus pacing period, and below SR Release is plotted against the pacing period. Black represents odd beats, and cyan represents even numbered beats. Electromechanically discordant alternans is present when the major cause of instability is a steep SR release slope. Figures are from Ref. [44].

Electromechanically discordant alternans also occurred when the SR release function and APD restitution curve were both steep [44]. Also note that in cases where electromechanically discordant alternans is observed, concordant alternans always precedes DA as the pacing period becomes more rapid. Sometimes this transition between CA and DA can happen more than once, as will be discussed in Section 3.11.

3.8 Bistability and Quasiperiodicity

Conduction blocks and skipped beats can produce periodic rhythms, which is believed to be a result of phase-locking. This rate-dependent failure of activation can lock into a stable rational ratio of two independent frequencies (1:2, 3:2, 3:4), and is called a Wenckebach rhythm. This phenomenon, also termed bistability, occurs when two different rhythms can be observed under the same conditions and can originate from a saddle-node bifurcation [44]. For a high enough SR uptake rate, a transition to alternans is accompanied by a saddle-node bifurcation that produces three steady-state solutions, where two fixed points are stable and the third is unstable.

In Figure 3.13, when a ventricular cell is periodically paced with decreasing period in a model produced by Yehia et al., a transition from 1:1 to 2:1 occurs when the period is decreased to 415 ms from 420 ms [56]. In order to return to a 1:1 rhythm, it was necessary to increase the period back up to 445 ms, a significantly higher period than was necessary to change rhythms in the other direction. This phenomenon is known as hysteresis.

A more complex situation is when the ratio of stimuli to responses becomes irrational, which produces quasiperiodic behavior. An example of quasiperiodicity is shown in Figure 3.15. In Shiferaw et al., quasiperiodic oscillations are driven by calcium instability in the calcium transient and voltage instability in the APD and have a phase and Hopf frequency that varied with the L-type calcium current recovery (τ_f, inactivation gate time constant) and the value of the SR release slope (u) [51].

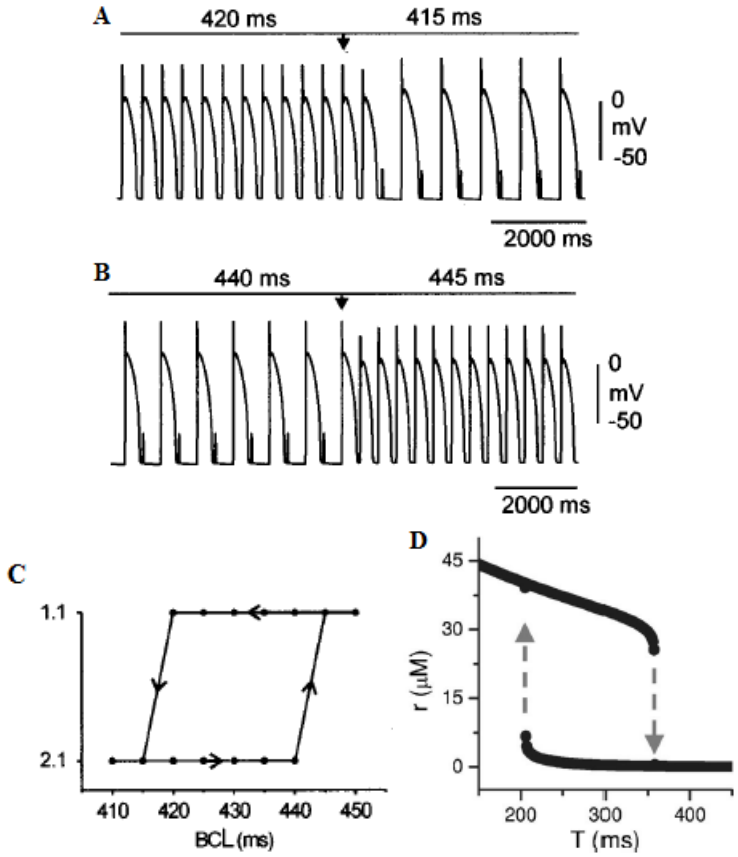

Figure 3.13: A) Hysteresis in the transition from between 1:1 and 2:1 rhythms. B) Hysteresis in the transition between 2:1 and 1:1 rhythms. The arrows indicate the beginning of the first cycle of the next pacing period. C) Diagram of hysteresis loop. Figures A, B, and C are from Ref. [56]. D) Hysteresis observed in the release of calcium from the SR observed by Qu et al. in Ref. [44] Dashed arrows indicate the discontinuous jumps as the period increases or decreases.

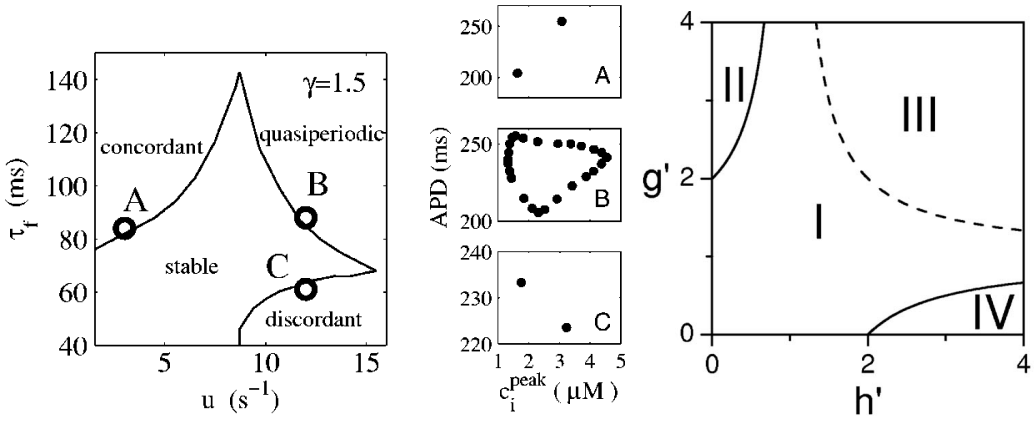

Figure 3.14: Left: Stability boundaries and unstable behaviors for negative voltage-calcium coupling (exponent above 1, $\gamma = 1.5$ in Ref. [51]). Electromechanically CA occurs when τ_f is dominant, causing voltage alternans. Alternatively, when u is dominant electromechanically DA can appear, driven by calcium alternans. For high enough values of τ_f and u, quasiperiodic behavior can be observed. Further out from the boundary, higher order rhythms and chaos are observed. Examples of these behaviors along the stability boundary are given to the right via plots of peak myoplasmic calcium concentration versus APD [51]. Right: Stability boundaries and instability regions as a function of h', the rate of calcium uptake into the SR and g', the rate of calcium release from the SR (analogous to the SR release slope). Region I is stable, and regions II and IV exhibit alternans and irregular dynamics. Region III is bistable. Figure is from Ref. [44].

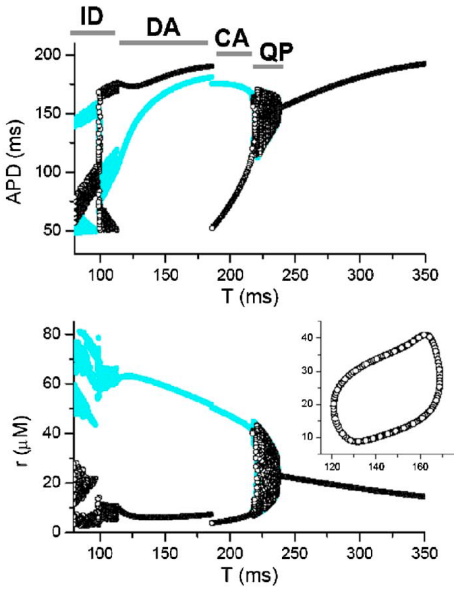

Figure 3.15: Bifurcation diagram for negative voltage-calcium coupling ($\gamma < 0$ in Ref. [44]), when voltage is primarily driving the instability. Above, APD is plotted versus pacing period, and below SR release is plotted against the pacing period. Black represents odd beats, and cyan represents even-numbered beats. An example of the quasiperiodic behavior observed is displayed in the inset of the lower diagram. The behavior of the system transitions from quasiperiodicity (QP) to concordant alternans (CA), followed by discordant alternans (DA) and chaos (irregular dynamics, ID). Figure is from Ref. [44].

3.9 Chaos

In dynamical systems, one of the most common routes to chaos is via a period-doubling bifurcation in systems with a monotonic APD restitution curve [49], or a Feigenbaum cascade (cascade of period-doubling bifurcations) when a biphasic APD restitution curve is utilized [52]. Other routes to chaos have been proposed, though, including intermittency [28, 51] and quasiperiodic behaviors leading to chaos [28, 44, 51]. At the tissue level, spatiotemporal chaos can be brought about by spiral breakup of action potential waves [32].

Chaos was observed in Ref. [49] when the SR release dependence on SR load was steep (see Fig. 3.8). In Ref. [51], Shiferaw et al. found that, given a positive coupling, it was only possible to achieve instability through concordant alternans, for which a series of period-doubling bifurcations results in chaos. Figure 3.16 shows a bifurcation diagram where the dynamics undergoes multiple period-doubling bifurcations that lead to chaos.

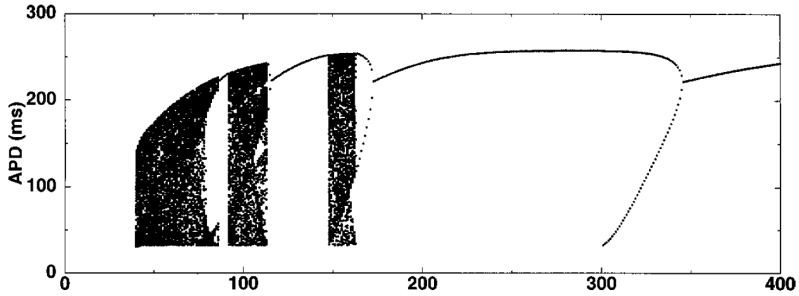

Figure 3.16: Bifurcation diagram of APD dynamics as a function of the cycle length, generated by a steep APD restitution curve from Ref. [28]. As the cycle length is decreasing a period-doubling bifurcation occurs, due to a slope above 1 of the restitution curve. Following the bifurcation, 2:1 conduction block occurs, supplanted by another period-doubling bifurcation, higher-order conduction blocks, and chaotic behavior.

3.10 Subcellular Alternans

It is well known that instability in intracellular calcium cycling can be responsible for cardiac alternans seen at the level of the whole cell. The degree of the connection, if any between subcellular alternans and whole-cell alternans has been investigated. One process by which subcellular alternans is generated has been proposed to be calcium waves within a cardiac myocyte. Diaz et al. suggest that the release of calcium from the SR propagates as a calcium wave [15]. Once a RyR channel is triggered by myoplasmic calcium, its own release of calcium from the SR can trigger nearby ryanodine receptors, signalling those channels to release calcium, and so on. The amplitude of these releases can drastically change from beat to beat during alternans, so the calcium released by RyR channels and sensed by nearby RyR channels varies as well [15]. Another explanation could be that an exceptionally large release of calcium from the SR could make RyR channels recover more slowly, such that their open probabilities are significantly reduced for the next stimulus

compared to RyR channels that were unrecruited during the previous excitation. Blatter et al. noted during experiments that when two adjacent regions in a myocyte were out of phase, steep diffusion gradients were observed between the neighboring regions, which caused the propagation of calcium waves to be delayed [5]. Shiferaw and Karma researched another means to subcellular calcium alternans, similar to a Turing instability observed in reaction-diffusion systems [50]. The analogy to Turing patterns is that the voltage acts as an inhibitor that diffuses faster than a short-range activator like intracellular calcium in cardiac cells.

Two crucial requirements of a Turing instability were that alternans must be caused by an instability in calcium cycling within the myocyte, and that the overall coupling between voltage and calcium (more specifically, voltage to calcium and vice versa) must be negative overall [50].

3.11 Transitions Between Spatially Concordant and Discordant Alternans

Although alternans has been shown in models and experiments to develop first as concordant alternans and then evolve to discordant alternans as the pacing cycle length is decreased [42, 44], followed eventually by conduction block (see Figure 3.17). Gizzi et al. have shown that this standard transition between concordant and discordant alternans is not necessarily always the case [22]. As shown in Figure 3.18, an additional recurrence of concordant alternans developed after a range of cycle lengths where discordant alternans was presented, and for some cases, another region of discordant alternans appeared following the second concordant alternans region.

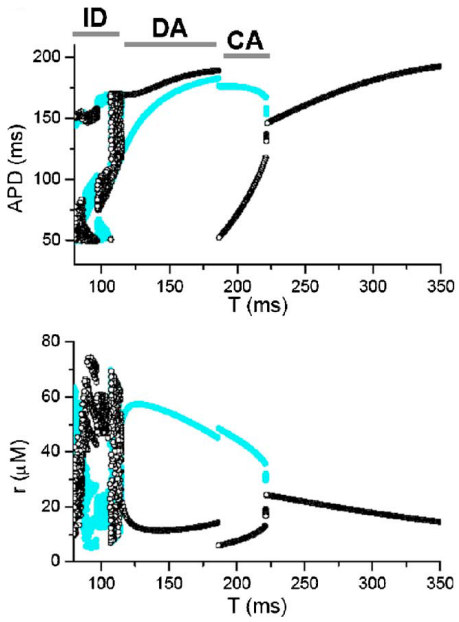

Figure 3.17: Bifurcation diagram for negative voltage-calcium coupling ($\gamma < 0$ in Ref. [44]), when voltage and calcium are both driving instability. Above, APD is plotted versus pacing period, and below SR release is plotted against the pacing period. Black represents odd beats, and cyan represents even numbered beats. As the pacing period decreases, electromechanically concordant alternans is followed by discordant alternans after conduction block. Irregular dynamics (chaos) occurs for even smaller pacing periods. Figures are from Ref. [44].

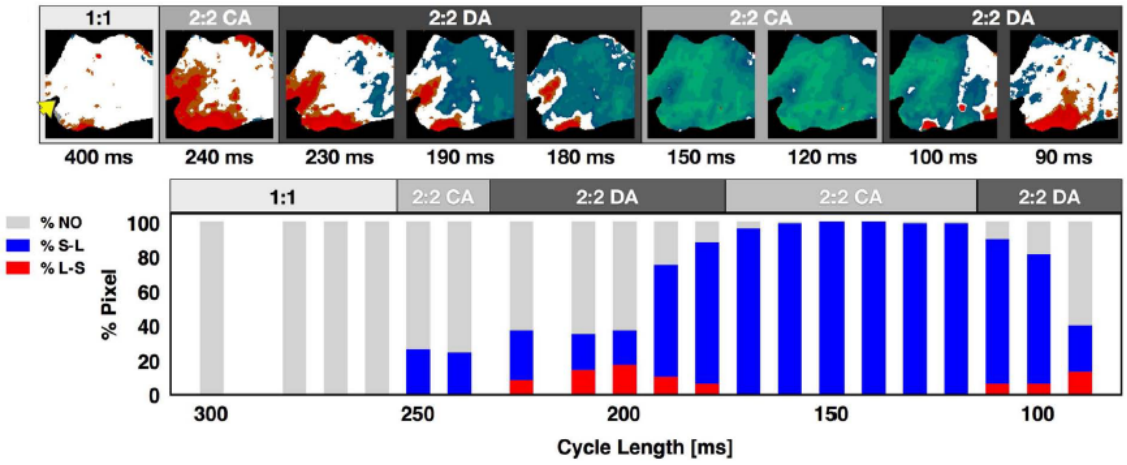

Figure 3.18: Transition from concordant alternans (CA) to discordant alternans (DA), then back to CA and again to DA was observed in cardiac tissue via optical mapping experiments as the CL decreased. Alternans maps for given cycle lengths (CL) are shown, with gray pixels representing no alternans, blue pixels representing alternating behavior with short then long APDs, and red pixels representing alternating behavior with long then short APDs. The yellow arrow indicates the pacing site. Figure is from Ref. [22].

Shiferaw et al. developed an intracellular calcium cycling model of a rabbit myocyte [49] that exhibited alternans behavior, as well as a cascade of period-doubling bifurcations that led to chaos. This particular model is the one we will be working with in this paper and implementing a delay-differential equation into. We will discuss this model and its results in detail in Sections 4 and 5.

Chapter 4

Methods and Implementation

4.1 Overview of Delay-Differential Equations

Delay-differential equations (DDEs) are similar to ordinary differential equations (ODEs), but differ primarily in that the derivative at any time depends on the solution at one or more previous times. The simplest form of a DDE is one with *constant delays*,

$$y'(t) = f(t, y(t), y(t-\tau_1), y(t-\tau_2), \ldots, y(t-\tau_k)),$$

where the time delays (also called lags) τ_j are positive constants[1]. In a more general case, DDEs with *state-dependent delays* also can depend on the solution at a previous time ($\tau_i = \tau_i(t, y(t))$). Although the topic of delay-differential equations is not as well-studied as ordinary differential equations, it is an area of growing interest. DDEs are widely used in predator-prey models [6, 19, 54, 55] and other biological sciences including epidemiology [1, 6, 54]. A less-common usage of DDEs is in diffusion-reaction systems [9, 19, 30]. DDEs have been utilized in cardiac modeling before in a mechanical setting [8] and in electrophysiological models by Courtemanche et al. [13, 14], and Gottwald et al. [25, 26].

[1]Please note that for our purposes, we will use δ instead of τ, to eliminate any confusion between delays and time constants. Please also note that we will refer to delays in other papers by the variables assigned to them in those papers (generally τ).

Cavalcanti et al. studied the implementation of a delay in the feedback of the baroflex control, a receptor that monitors the arterial pressure of the heart [8]. The behavior of the system varied significantly with the delay and exhibited steady-state solutions and a Hopf bifurcation that produced spontaneous oscillations. For larger delays, the oscillations increased in complexity and followed a period-doubling cascade, which has been strongly identified as a route to chaos. Refs. [13, 14, 25, 26] modeled how pulses propagated in a ring of excitable media using a reaction-diffusion partial differential equation (PDE) derived from the ionic current equations by Beeler and Reuter [3]. Courtemanche et al. reduced the PDE in Refs. [13, 14] to an integral-delay equation, based on the physical mechanisms controlling pulse propagation in a ring of excitable tissue, shown in Equation 4.1. Namely, the relations between restitution and dispersion (conduction velocity restitution) with the recovery time (the time between the end of an excitation pulse and the initiation of the next pulse) are functions of a delay, where a larger delay corresponded to a longer recovery time. The value of the delay was derived from the restitution and dispersion curves generated from simulations of the PDE mentioned above. Essentially, Equation 4.1 is a conservation equation where the recovery time ($t_r(x)$) is equal to the circulation period ($c(t_r)$) minus the pulse duration ($a(t_r)$). An infinite-dimensional Hopf bifurcation occured when the restitution relation's slope was above 1, signalling a proclivity towards alternans behavior.

$$t_r(x) = \int_{x-L}^{x} \frac{ds}{c(t_r(s))} - a(t_r(x-L)) \tag{4.1}$$

Gottwald studied wave trains on a ring of excitable media using a delay-differential equation (Equation 4.2 is a normal form), where a delay represented the inhibiting effects of a wavefront catching up to another waveback [25, 26]. In Equation 4.2, X represents the pulse velocity, μ is a bifurcation parameter related to inhibition and refractoriness of excitable cardiac tissue, β_0 is the strength of the inhibitor, and $V(t-\tau)$ describes the effect of the previous pulse's inhibition. Gottwald was able to recreate the Hopf bifurcation, which also was linked to alternans behavior. He used a more complicated DDE, basing it on the interaction of a propagating pulse with the "inhibitor" of the preceding pulse. Gottwald presented a normal form for the DDE that exhibited a rich bifurcating behavior, including an inhomogeneous pitchfork bifurcation and saddle-node

and subcritical Hopf bifurcations, which collided to produce the unfolding of a Bogdanov-Takens point of co-dimension 2. Gottwald also produced a condition for alternans ($\beta\tau \geq 1$) where β corresponds to the inhibitor and τ is the delay, and both β and τ are constants. Another important discovery was that the Hopf bifurcation was *subcritical*, which disagreed with many sources [13, 14, 32] that have found *supercritical* Hopf bifurcations and period-doubling bifurcations in the context of alternans. To the best of our knowledge, these are the only applications of DDEs to cardiac modeling.

$$\frac{\partial X}{\partial t} = -\mu - gX^2 - \beta_0 V(t-\tau) \tag{4.2}$$

Our main motivation for using delay-differential equations in this study is that the diffusion process through the SR can be described as a delay between the uptake of calcium ions into the NSR and its availability for release from the JSR. The current approach to modeling diffusion through the SR is via a relaxation ordinary differential equation that utilizes a time constant that is not precisely known. We believe our alternative formulation of this diffusion process could present new insights into possible instability mechanisms in the calcium cycling dynamics that other models currently do not, and varying the delay in our model could correspond to clinical situations. We present a calcium cycling model in Section 4.2, and propose our alternative delay-differential equation formulation for the diffusion of calcium through the SR.

Our application of DDEs will be to calcium cycling and on the intracellular level in ventricular myocytes, both novel applications of DDEs to cardiac modeling. In the intracellular calcium cycling model presented by Shiferaw et al. (Ref. [49]), we will implement a delay into the original system of ODEs to describe the diffusional flow of calcium ions through the NSR-JSR network. The delay also could be interpreted as the recovery of RyR after the release of calcium from the SR, discussed in Section 4.3. This use of a delay is different in nature from previous applications, in that Courtemanche et al. [13, 14] used a delay to account for the changes in recovery time based on restitution curves of the action potential and conduction velocity, and Gottwald et al. [25, 26] utilized a delay to describe the inhibiting effects of neighboring pulses traveling on a ring of excitable media.

Since the solution of DDEs at any point in time depends on prior solutions, a history function containing the previous solutions backwards beyond the largest delay back must be maintained and updated. This also means that an initial history function must be specified prior to solving the equation(s); initial history functions generally are constants. A simple comparison between an ODE and its delayed (corresponding DDE) solution is illustrated in Figure 4.2.

4.2 Model

The main system of equations that we use in this model describe the calcium concentrations in different areas within the myocyte and the release current, from Ref. [49].

$$\begin{aligned}\frac{dc_s}{dt} &= \beta(c_s)[\frac{v_i}{v_s}(I_r(t) - \frac{(c_s - c_i)}{\tau_s} \\ &\quad - I_{Ca}(c_s, V) + I_{NaCa}(c_s, V)) - I^s_{trpn}] \qquad (4.3)\\ \frac{dc_i}{dt} &= \beta(c_i)(\frac{(c_s - c_i)}{\tau_s} - I_{up}(c_i) - I^i_{trpn}) \qquad (4.4)\\ \frac{dc_j}{dt} &= -I_r(t) + I_{up}(c_i) \qquad (4.5)\\ \frac{dI_r}{dt} &= gI_{Ca}(t)Q(c'_j) - \frac{I_r(t)}{\tau_r} \qquad (4.6)\\ \frac{dc'_j}{dt} &= \frac{c_j - c'_j}{\tau_a} \qquad (4.7)\end{aligned}$$

We are interested in altering this model by describing the diffusional flow from the NSR to the JSR via a DDE, rather than the "relaxation" ODE currently used in the model. Relaxation ODEs are prevalent throughout many fields of mathematical modeling, and use a time constant (usually denoted by τ) that controls how fast a value approaches its steady state. Our approach will be to use a simple first-order linear DDE, utilizing a constant delay instead of a time constant. Equation 4.7 is replaced by the following equation

$$\frac{dc'_j}{dt} = c_j(t) - c_j(t - \delta_j), \tag{4.8}$$

where the delay δ_j can be varied, much like the τ_a time constant used in Refs. [38, 49]. We use the subscript j for the delay because the delay is applied to the SR concentration which also has the subscript j, and in anticipation of utilizing more delays in the system of equations (Equations 4.3 - 4.7), even though δ_j is the sole delay implemented in our preliminary research shown in this document. The physical representation of this time constant (and our delay) can be interpreted in different ways. We will discuss those interpretations in the next section.

Equation 4.9 is the release function in Equation 4.6, and is a piece-wise defined relation used in Ref. [49] to describe the all-or-none response of calcium release from the SR. The SR release slope u is an adjustable constant, and s is fixed by the condition that the release function be continuous. The steepness of the SR release slope played a major role in developing alternans and chaos in Ref. [49]. The importance of the SR release slope in the calcium dynamics and its effects will be discussed further in Section 5.3.

$$Q(c'_j) = \begin{cases} 0 & 0 < c'_j < 50\mu M \\ c'_j - 50 & 50\mu M \leq c'_j \leq 115\mu M \\ uc'_j + s & c'_j \geq 115\mu M \end{cases} \tag{4.9}$$

4.3 Physiological Interpretations of τ_a and δ_j

The τ_a constant used in Refs. [38, 49] is the relaxation time and corresponds to the average time it takes for a calcium ion somewhere in the SR (generally the NSR) to diffuse into a JSR compartment. Since there has been no experimental measurement of this quantity, the exact value that τ_a should be is uncertain. The NSR is a complex network of tubules, and thus determining a single value that accurately describes the flow of Ca^{2+} ions from

anywhere in the NSR also is difficult. The value of τ_a ranged from 1 to 100 ms in Ref. [49]. Increasing the value of τ_a subsequently increased the amount of calcium released from the JSR compartments during CICR. During SR calcium release, recruited JSR compartments empty calcium ions into the submembrane space and cause the overall concentration in the SR to drop below the calcium concentration in unrecruited JSR compartments. Since the unrecruited JSR compartments are not releasing calcium, some calcium flows back into the SR and diffuses into recruited JSR compartments and is released from the SR. Because the release function defined in Ref. [49] was a monotonically increasing function, a longer delay time allows more calcium to be drained from the SR because it takes longer for the calcium concentration to equilibrate throughout the SR.

Despite the effect of increasing τ_a, the total change in released calcium was not large enough to overcome the diffusional processes out of the submembrane space, since the pacing periods investigated were large enough to compensate for the additional calcium. At the time, Shiferaw et al. concluded that although τ_a did contribute to calcium instabilities it was not crucial in generating alternans and chaos and that the dependence of SR release on SR load was the dominating factor in producing these behaviors [49]. Figure 4.1 demonstrates the effect of increasing τ_a on calcium efflux from the SR.

Mahajan et al. determined that τ_a played a critical part in the genesis of alternans behavior in their calcium cycling model [38]. They also provided an additional interpretation of the relaxation constant τ_a. They proposed that τ_a could correspond to the refractoriness of SR calcium release channels (recovery of RyR) after CICR. Given this explanation, c_j' would represent a refractory period regulated directly by c_j', as opposed to representing the calcium concentration in a space (specifically the average JSR compartment concentration).

In our implementation, we will vary the delay δ_j and analyze the dynamical consequences.

4.4 Numerical Methods

To solve this system numerically, we used a forward Euler numerical scheme similar to that utilized in Ref. [13]. Solving a DDE with this type of method comes with a few additional

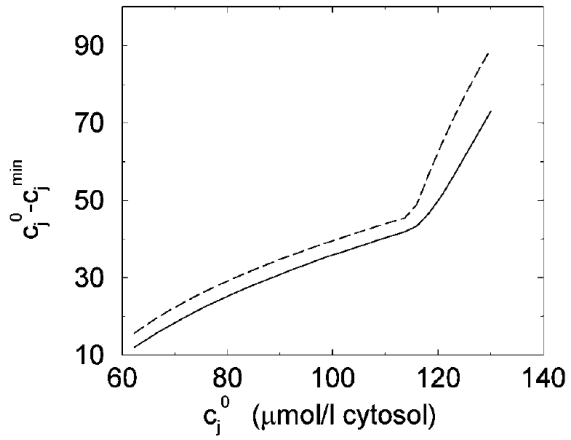

Figure 4.1: Dependence of maximum SR calcium flux on initial SR calcium load. The solid line corresponds to a relaxation time of $\tau_a = 1$ ms, and the dotted line corresponds to a relaxation time of $\tau_a = 100$ ms. More calcium was released from the SR for all initial JSR loads when the relaxation time τ_a was long opposed to a short relaxation time. Figure is from Ref. [49].

considerations. First, we used a simple forward numerical scheme where the solution evolves each time from the previous step, but there is a delay in the differential equation so the solution must reference an earlier point in time in addition to the most recently solved point. Because of this, we chose a minimum discretization step and restricted the possible delay to an integer multiple of the discretization step in order to solve the DDE numerically. A delay of zero is allowed; this would simply make the DDE an ODE. These restrictions allow for a simple adaptation of the forward Euler numerical method and prevent any need for interpolation between previously solved points during numerical integration of the DDE.

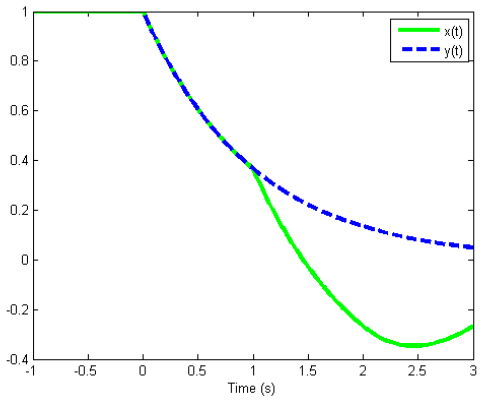

Figure 4.2: Solutions to a simple ODE and its delayed version ($\dot{y} = -y(t), \dot{x} = -x(t-\tau), \tau = 1$) with a time step of .01 seconds. The DDE solution is plotted from $t = -1$, to illustrate the constant initial history function. Notice that the delayed solution continues to decrease below a value of zero (the steady-state value), whereas the ODE solution converges to zero from above.

Maintaining the history while integrating the system involves several steps. Solving any type of DDE requires an initial history function, far enough back in time before $t = 0$ so that the largest delay can access it (e.g., a delay of 2 ms requires an initial history function that goes back at least to $t = -2$ ms). The most common initial conditions used in ODEs are also the most commonly used initial history functions for DDEs: constants. For DDEs, we simply provide a constant as the initial value that extends as far back in time as necessary. We will use constant initial history functions in obtaining our numerical solutions. Once the time has passed any delay in the system of equations, the solver will not reference the initial history function anymore. Instead, after solving the system at each time step, a history function is updated with the previous solutions of the delayed value back up to the value of the longest delay. Constant initial conditions and histories are common in cardiac simulations, under the assumption that all numeric values have been at diastolic levels well before the first depolarization occurs in simulations. Alternatively, time-varying values obtained from steady-state pacing can be used as initial histories as well.

4.5 Method for Determining Calcium Peaks

Numerical simulations performed for this study were done for a total time of 100 seconds in all cases, to ensure that any periodic behavior or irregular dynamics were not transient in nature unless noted otherwise. To determine whether periodic behavior was present, we developed a backward-searching algorithm. Starting from the end of the simulation, the algorithm proceeds backwards through time to find the values of the peak (or minimum) myoplasmic concentrations. Upon finding a maximum (minimum) its value is recorded and is compared to the next peak value found. As the algorithm continues to progress backwards, it terminates as soon as any pattern is discovered and returns the period calculated. For example, if 1:1 behavior was simulated, the last peak would equal the second-to-last peak value. For higher periodicities, once a pattern of peak values was repeated, the number of peaks between the first repetition of peak values is the period.

Chapter 5

Results

Alternans and chaos (fibrillation) are important physiological behaviors observed in cardiac models and experiments. Our goal was to investigate how delay-differential equations could be used in cardiac modeling to produce these relevant dynamics in the setting of a mathematical model. We have done this by modeling the diffusion of calcium through the SR using a delay-differential equation. We incorporated a DDE into the calcium cycling model presented in Ref. [49] and aimed to produce alternans and chaos behaviors seen in Ref. [49] by changing the value of the delay implemented. To study the dynamics that arose from incorporating Equation 4.8 into the system of ODEs, we conducted 100-second simulations of the calcium dynamics and then discerned between steady-state, periodic and chaotic behavior by the process outlined in Section 4.5. We were able to produce all of the significant behaviors shown in Ref. [49], including alternans behavior and chaos. We also studied the effect of the SR release slope on the system, and developed conditions for when the dynamical system will be stable (producing steady-state, and consistent periodic solutions), and conditions for which it will be unstable (chaotic). We studied how the value of δ_j affects the system for a fixed pacing period, and vice versa. Then, we determined threshold values of δ_j at which alternans, and chaotic behavior appeared. We also present the progression of peak myoplasmic calcium dynamics as the value of δ_j was increased, showing transitions from steady-state to periodic, and eventually chaotic behavior. For large enough delays, the complexity of progression was significantly advanced.

5.1 Model Validation

To validate our incorporation of a DDE into a model of intracellular calcium cycling in cardiac myocytes, we analyzed some of the dynamics and physiological quantities produced in our model with the inclusion of a DDE by comparing our results to other models of calcium cycling and cardioelectrophysiological experiments in the literature (Refs. [11, 38, 49]). We compared our model with the results of others in Figures 5.1, 5.2 and 5.3.

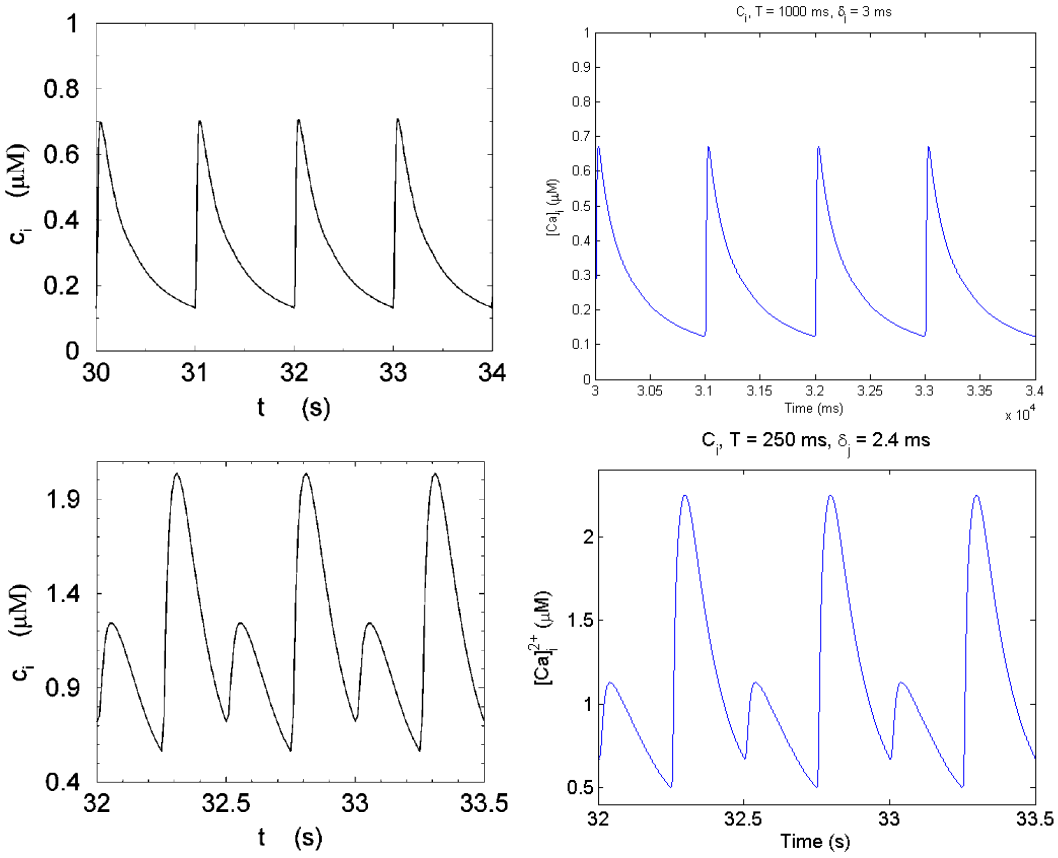

Figure 5.1: Top figures: Plots of myoplasmic calcium concentration (c_i) versus time for T = 1 s, from Ref. [49] on the left, and our model on the right (δ_j = 3 ms). Bottom figures: Plots of myoplasmic calcium concentration versus time for a more rapid pacing period (T = 250 ms), again from Ref. [49] on the left, and our comparison on the right (δ_j = 2.4 ms). Plots are of steady-state time courses of c_i in all cases.

Our results are in good qualitative agreement with the numerical simulations of the model from Ref. [49], as shown in Figure 5.1. The calcium transients for moderate delays (we used $\delta_j = 3$ ms in Figure 5.1) resulted in slightly smaller calcium peaks than in Ref. [49] under the same conditions. Our comparison with Ref. [49] at a faster pacing rate also qualitatively agreed, but in this case the lower peaks were approximately identical while the larger peaks acheived a marginally greater maximum (2.2 μM as opposed to 2 μM). We compared our results for the same time frame as it is chosen in Ref. [49] to show that steady-state was achieved by the same amount of time.

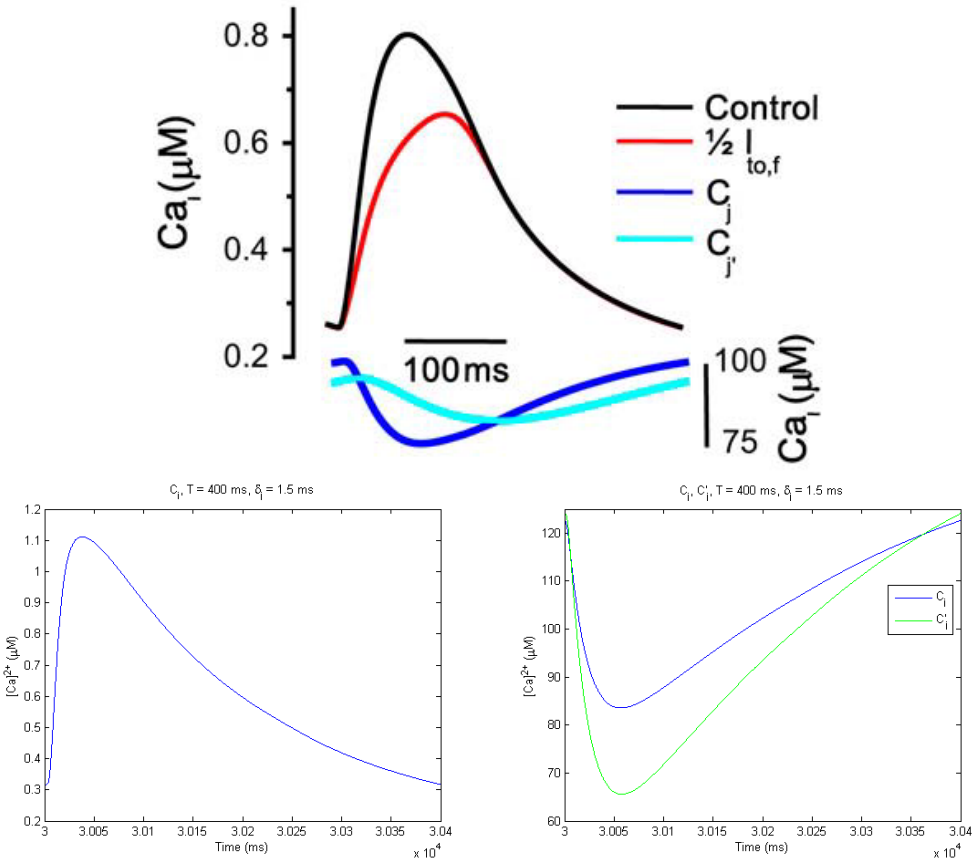

Figure 5.2: Top: Plots of calcium transient (bulk myoplasmic concentration, black), $[Ca]^{2+}{}_{SR}$ (blue), and $[Ca]^{2+}{}_{JSR}$ (cyan) for a pacing period of T = 400 ms from Ref. [38]. Note that the scale is much higher for the SR and JSR calcium concentrations (75-100 μM) than the calcium transient. Bottom figures: Plots of the myoplasmic calcium concentration (left) and the SR (C_j, blue) and JSR (C'_j, green) concentrations (right) from our model. The pacing period is also T = 400 ms, and $\delta_j = 1.5$ ms.

Figure 5.2 demonstrates that our simulations of the bulk myoplasmic calcium concentration, SR and JSR calcium concentrations were in relatively good agreement with the model results produced by Mahajan et al. in Ref. [38]. The calcium transient behaved similarly, although showing a larger peak in myoplasmic calcium (1.1 μM compared to .8 μM in Ref. [38]). The time courses of the SR and JSR concentrations were similar, although initial calcium levels were set higher in Ref. [49] (120 μM) than in Ref. [38] (100 μM).

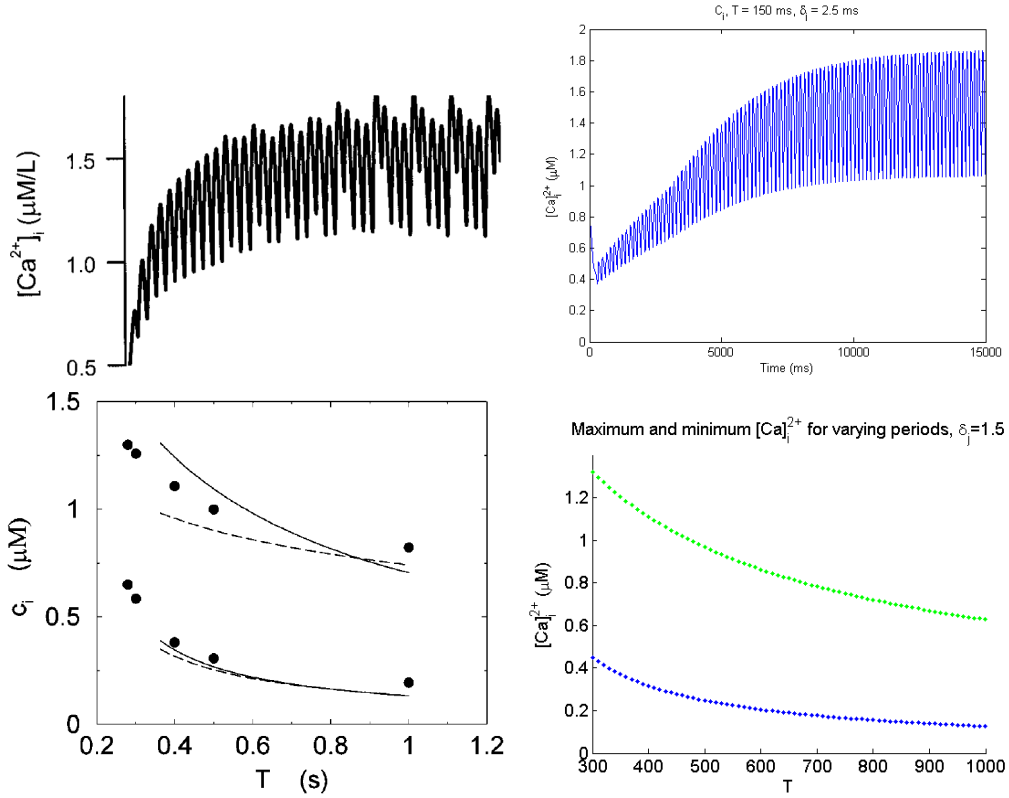

Figure 5.3: Top figures: Myoplasmic calcium concentration from mathematical model, from Ref. [11]. Pacing was fixed at $T = 150$ ms (left). Simulation of myoplasmic calcium for first 15 s, pacing at the same rate ($T = 150$ ms), and $\delta_j = 2.5$ ms (right). Bottom figures: Maximum and minimum myoplasmic calcium levels for a range of periods (model results are the solid lines, filled circles are experimental data points from Ref. [11], and the dotted lines are results when intracellular sodium was fixed at 10 mM) from Ref. [49] (left). Right: Plots of maximum and minimum c_i values for a range of periods generated from our model (every 10 ms between $T = 300$ and $T = 1000$ ms).

Additionally, in Figure 5.3 we compared our simulations of the calcium transient with computed results by Chudin et al. in Ref. [11]. For rapid pacing ($T = 150$ ms), a delay of 2.5 ms produced results similar to Chudin et al. After 15 s of simulation, the range of values (1.8 μM maximum, 1 μM minimum) appeared to be in good agreement with simulations from Ref. [11]. Note that the initial condition appeared to be about .5 μM in Ref. [11], where we used the initial value given by Shiferaw et al. in Ref. [49] (.1 μM). We also compared maximum and minimum values of the bulk myoplasmic calcium concentrations with Ref. [49] for a range of pacing periods. For a delay of 1.5 ms, the graphs were nearly identical across all periods simulated.

For a fixed pacing period, increasing the delay produced alternans. For small delays ($\delta_j = 1$ ms), stable period-1 behavior is achieved. As the delay increased, alternans behavior appeared. As we continued to increase the delay, the amplitude of alternans grew, and then shrunk as the delay increased from 3 ms to 6 ms. Eventually, for a large enough value of δ_j (7 ms), period-4 behavior occurred, as small notches began to appear between the two relatively larger calcium peaks. Finally, at a delay of 8 ms, chaos appears in the calcium dynamics. Note that the y-axis scale changes; the maximum calcium peak amplitude increased along with the value of the delay. A sample progression of the calcium dynamics is shown as the delay is increased in Figure 5.4.

5.2 Alternans

Alternans has been identified as a predecessor to instabilities in cardiac systems in both experiments and models. Physiological models that reproduce alternans behavior in the context of calcium cycling could help to better understand the source of dynamical instabilities. In our model results, we were able to produce alternans behavior that was similar to results in Ref. [49].

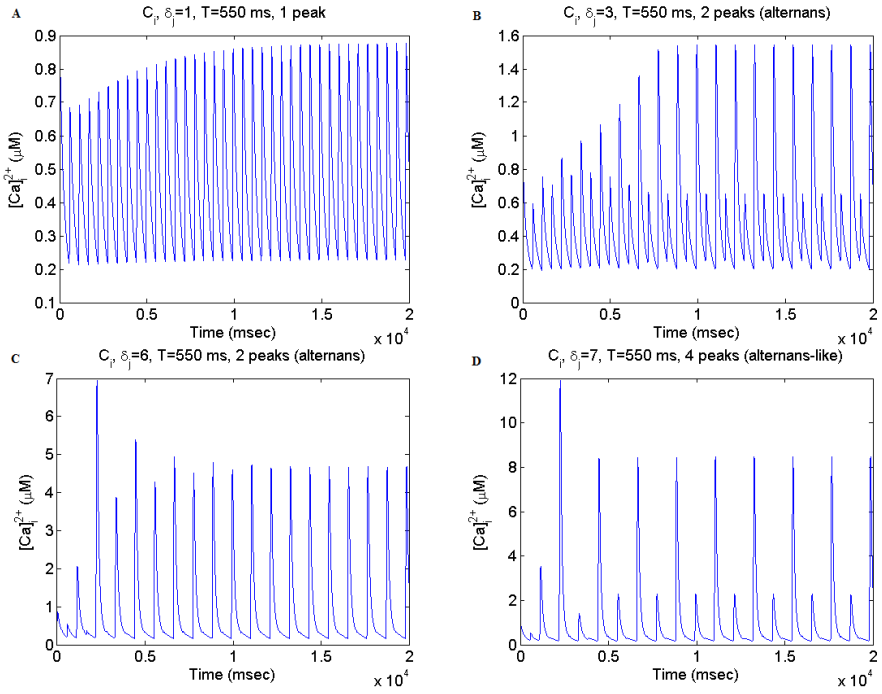
A
C_i, δ_j=1, T=550 ms, 1 peak
B
C_i, δ_j=3, T=550 ms, 2 peaks (alternans)
C
C_i, δ_j=6, T=550 ms, 2 peaks (alternans)
D
C_i, δ_j=7, T=550 ms, 4 peaks (alternans-like)
[Ca]_i^2+ (μM)
Time (msec)
x 10^4

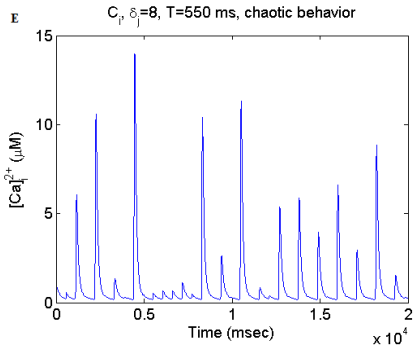

Figure 5.4: Progression of myoplasmic calcium concentration dynamics with increasing delay. Note that the maximum peak values increase with increasing delay, and the y-axis scale changes accordingly. The first 20 seconds of simulation are shown, since steady-state solutions are achieved within that time frame, or there is chaotic behavior. A) Stable, period-1 behavior for a delay of 1 ms. B) Persistent alternans behavior is observed with a delay of 3 ms. C) A large spike in myoplasmic calcium precedes alternans behavior at a time of about 2.5 s. Delay of 6 ms is used; the amplitude of alternans is significantly smaller than that of B). D) At a delay of 7 ms, the amplitude of alternans is very large, and small notches in c_i begin to form, presenting an alternans-like period-4 behavior. E) Chaos occurs at a delay of 8 ms, with extremely large peak values of myoplasmic calcium concentration.

In comparison to Figure 3.8, we observed that alternans initiated at a higher period (420 ms compared to 320 ms), but also ceased at a period of 200 ms in Figure 5.5. For this particular delay ($\delta_j = 2.2$ ms), the amplitude of alternans was larger and the peaks were at more extreme values than observed in Ref. [49].

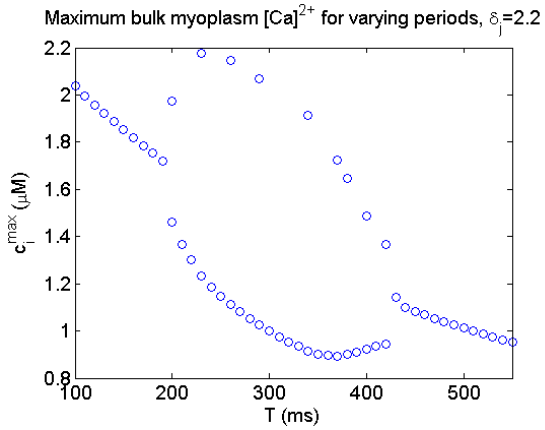

Figure 5.5: Plot of peak myoplasmic calcium concentrations for varying periods. The delay was fixed at 2.2 ms. Alternans behavior occurred for a range of about 200 ms to 420 ms.

Alternans behavior was not observed for any pacing periods when $\delta_j < 2.1$ ms. For delay values around 2.15 ms (2.1 - 2.18), we observed two separate intervals of periods where alternans occurred. As shown in Figure 5.6, period-1 behavior occurs for a small interval of periods of about 10 ms. We found this transition reminiscent of the transitions between spatially concordant and discordant alternans seen in Figure 3.18. Also note that this result has not been observed in other models of intracellular calcium cycling but could be evidence of a period-halving bifurcation (period-doubling reversal), suggested by Watanabe et al. [52].

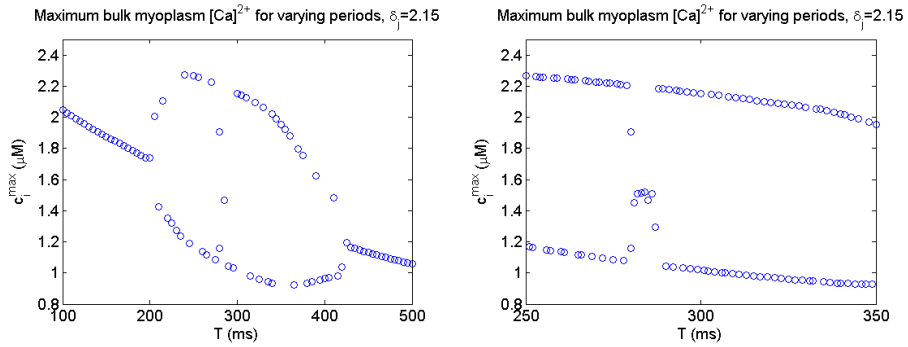

Figure 5.6: Alternans appears, disappears and reappears as the pacing period decreases. The plot to the right is the same simulation, but focused on the area where 1:1 behavior briefly returns.

5.3 Chaos

Fibrillation observed at the tissue level is thought to be dynamically chaotic, and cardiac alternans often precedes fibrillation. We also observed chaos in our ODE-DDE calcium cycling system of equations for high values of δ_j. A series of period-doubling bifurcations led to chaos, as shown in Figure 5.7. From our results, we believe that calcium instabilities observed could incite chaos and alternans, although this would need to be addressed specifically to determine the magnitude of influence of calcium on the action potential dynamics. Figures 5.8 and 5.9 show bifurcation diagrams for peak myoplasmic calcium for a fixed period and varying delay.

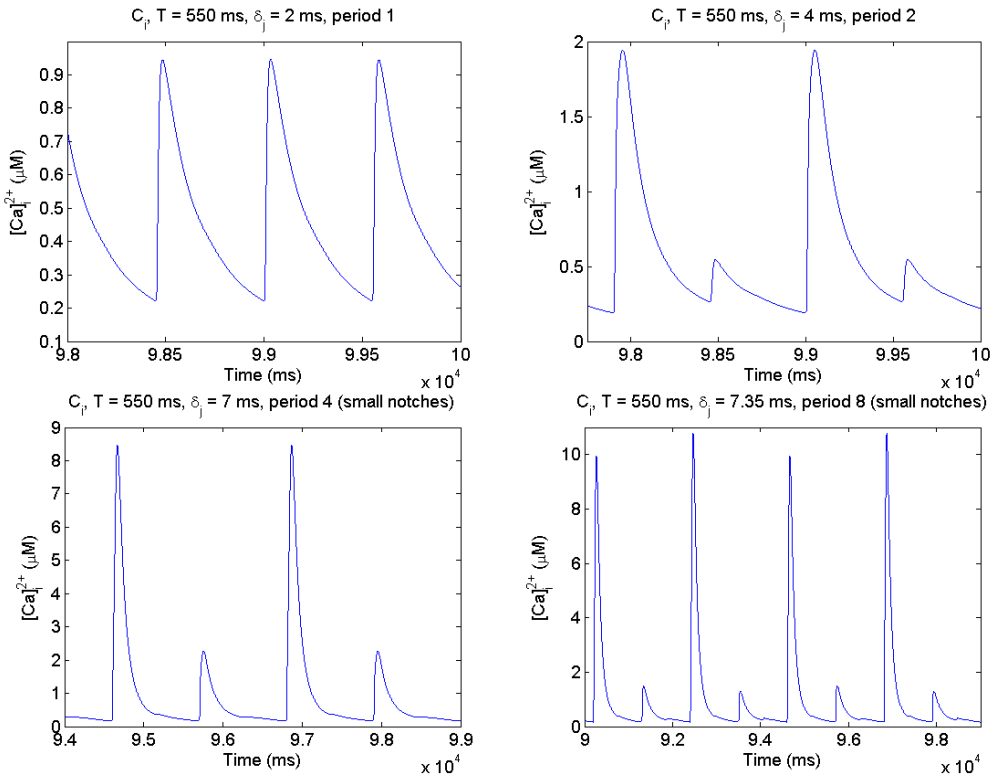

Figure 5.7: Example of period-doubling behavior seen as the value of δ_j increases, $T = 550$ ms. The periodic behavior jumps from period 1, to 2, 4, and then 8 as the delay is increased. Note that for the period 8 graph, there are small but distinct peaks following the small spikes but before the larger spikes in myoplasmic calcium concentration.

Also note that a steep SR release slope ($u = 43.3\ \mu M/s$) was necessary to produce chaotic behavior in Ref. [49], but a steep slope was not necessary for chaos to occur in our numerical simulations. We used a physiologically normal SR release slope ($u = 11.3\ \mu M/s$) from Ref. [49] in Figure 5.8. This result is of particular interest because a steep SR release slope has been cited as a critical factor in producing alternans [4, 18, 38, 44, 49, 51] and potentially unstable behaviors such as chaos [44, 51, 49]. This may suggest that the delay between NSR uptake and JSR availability (or RyR recovery) may be able to produce alternans and higher-order dynamics despite a physiologically normal SR release slope. We will show results of myoplasmic calcium dynamics with a steep SR release slope as well in Section 5.4.

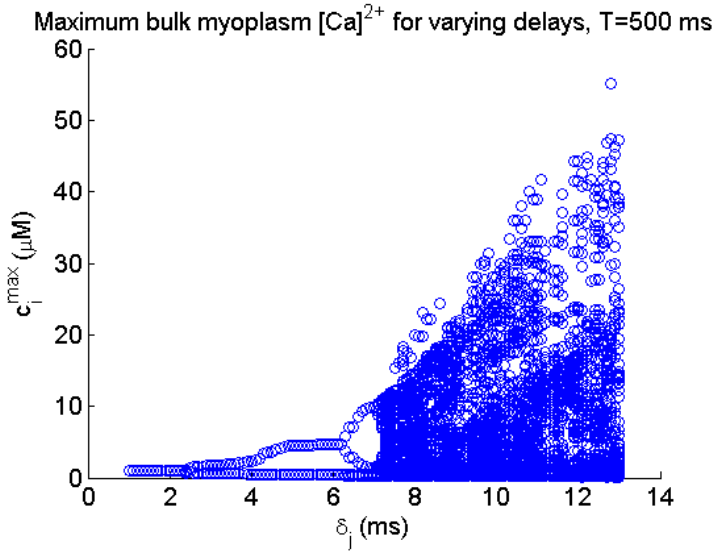

Figure 5.8: Peak bulk myoplasmic calcium for varying delays. The pacing period was held constant at $T = 500$ ms. As the delay is increased, the stable 1:1 rhythm evolves into alternans at a delay of 2.4 ms. Further on, the amplitude of alternans grows until the delay reaches 6 ms, after which higher-order periodicities and chaos are observed.

A bifurcation diagram for varying values of the delay, with the period fixed at $T = 150$ ms is shown in Figure 5.9. Compared to Figure 5.8, the dynamics were more complex. For $T = 500$ ms, once the delay was high enough to produce chaos, no other behaviors were observed for delays above 8 ms. But for a more rapid pacing period ($T = 150$ ms), three separate regions of chaos were evident at delays at or above 8 ms, and a broader range of periodicities were apparent for the periods simulated.

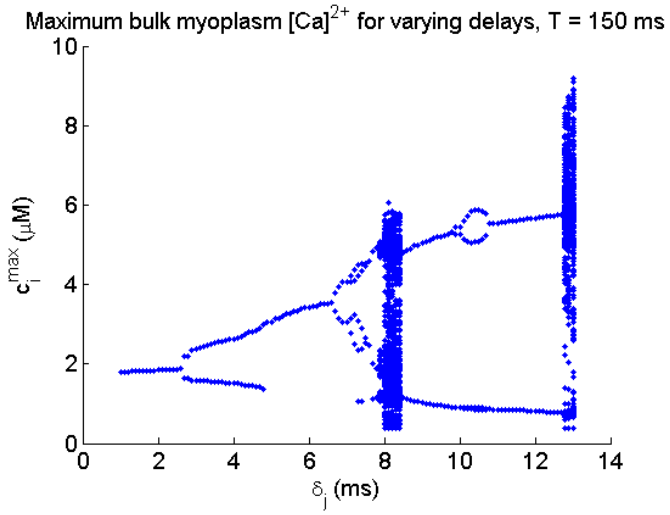

Figure 5.9: Bifurcation diagram of peak bulk myoplasmic calcium concentrations for varying delays, with the period held constant at 150 ms. Periods 1,2,4 and 3, and chaos are observed for particular delays. Three regions of irregular dynamics (chaos) exist, around delays of 8, 11, and 13 ms. The overall progression and appearance of these periods alongside return maps is displayed in Figure A.1.

The bifurcation diagram in Figure 5.9 shows similar transitions between periodic and chaotic behavior to the bifurcation diagram in Figure 3.16. There was also the presence of period-3 and other higher-order periodicities.

5.4 SR Release Slope

A steep SR release slope was the crucial factor in producing irregular dynamics within the myocyte in Ref. [49]. Although a steep SR release slope was not required to produce chaos in our model, increasing the SR release slope allowed more complex dynamics to occur for smaller delays than with a normal SR release slope, as Figure 5.10 shows. Note that alternans behavior appeared only when $\delta_j \geq .7$ ms (the lower bound for alternans behavior with a physiologically normal release slope was 2.1 ms).

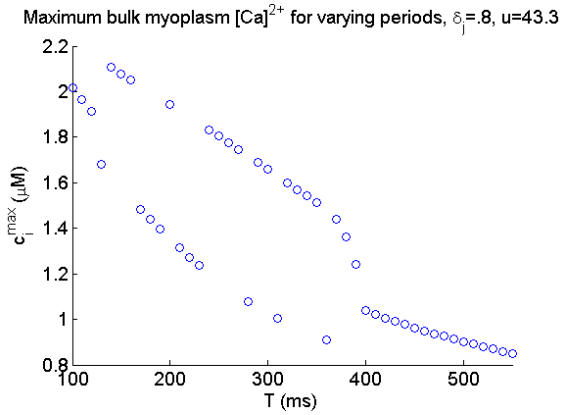

Figure 5.10: Plot of maximum bulk myoplasmic calcium content for varying periods, and a steep SR release slope (43.3 $\mu M/s$). Alternans behavior appeared for a smaller delay ($\delta_j = .8$ ms compared to 2.2 ms in Figure 5.5). The range of pacing periods over which alternans persisted was considerably larger than simluations with a normal SR release slope.

Transitions between stable and unstable behavior occurred in a similar fashion with a steep SR release slope as compared to a physiologically normal SR release slope (Figures 5.9 and A.1). A bifurcation diagram of the myoplasmic calcium dynamics with increasing delay and steep SR release slope are shown in Figures 5.11. As the delay was increased in Figure A.1, alternans behavior begins to appear a delay of .7 ms. Once δ_j reaches about 3 ms, alternans disappears, returning to stable period-1 behavior. For values of δ_j up to 3.5 ms, higher periodicities and chaos result. There is a short range of δ_j between 3.7 and 3.8 ms where periodic solutions briefly return before chaotic dynamics return. As the delay continues to increase, alternans appear again between delays of about 4.4 and 5.5 ms, before more complex periodicities lead to chaos initiated at $\delta_j = 6.3$ ms.

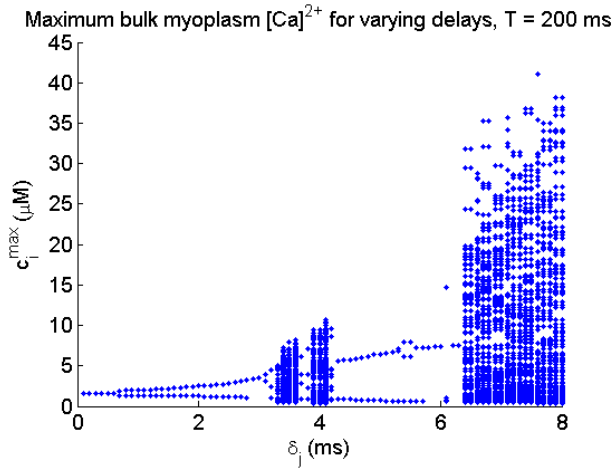

Figure 5.11: Plot of peak myoplasmic calcium for varying delays, and a steep SR release slope (43.3 $\mu M/s$) with the period held constant at 200 ms. Three regions of chaos occurred for smaller delays than in numerical simulations with a normal SR release slope. Three regions of chaos occurred around delay values of 3.5, 4, and 6.5 ms.

The progresssion into and of out chaotic dynamics in Figure 5.11 is shown in Figure A.2. A bifurcation diagram displaying dynamics between myoplasmic calcium and pacing period with a fixed delay is shown in Figure 5.12. Particular high-order periodicities observed at different pacing periods and delays with a steep SR release slope are shown in Figure 5.13.

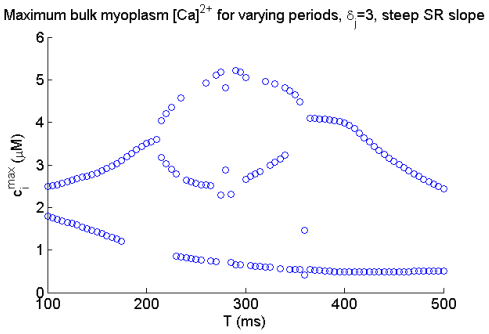

Figure 5.12: Plot of peak myoplasmic calcium values for varying pacing periods, and a steep SR release slope (43.3 $\mu M/s$). The delay was fixed at 3 ms. Periodic behavior of at least period 2 was seen for all pacing periods investigated (100 ms $\leq T \leq$ 500 ms), with the exception of a small range of periods around 200 ms where alternans disappeared. The presence of a period-3 solution also was apparent in this bifurcation diagram.

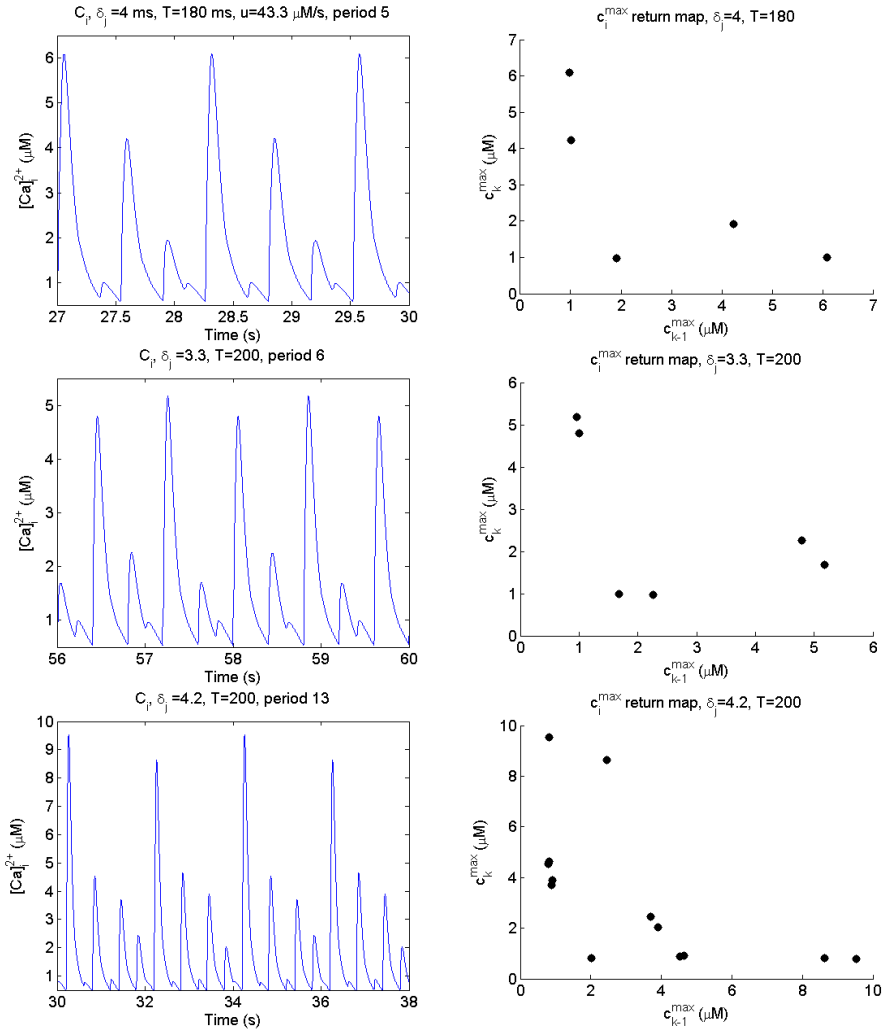

Figure 5.13: High-order periodicities (not powers of 2) are exhibited for varying periods and moderate delays when there is a steep SR release slope, including periods 5, 6, and 13. Pacing periods range from 180 ms (top) to 200 ms (bottom), and delays range from 3.3 ms to 4.2 ms (exact values are displayed in the title of each figure). Also note that the SR release slope was steep (43.3 $\mu M/s$). Corresponding return maps are on the right.

5.5 Conditions for Instability

Our ODE-DDE system of equations showed several transitions to and out of chaos, as seen in Figures 5.9, 5.11, and observed by Hastings et al. (Figure 3.16). Our goal was to develop conditions for when the calcium system would exhibit stable (periodic) behavior and chaos. Approximately-defined regions of stability and instability are shown in Figure 5.14. To determine these ranges, we conducted simulations and determined whether the myoplasmic calcium concentration was stable (periodic) or unstable (chaotic). We further divided the stable regions into period-1, alternans (period-2), and high-order periods.

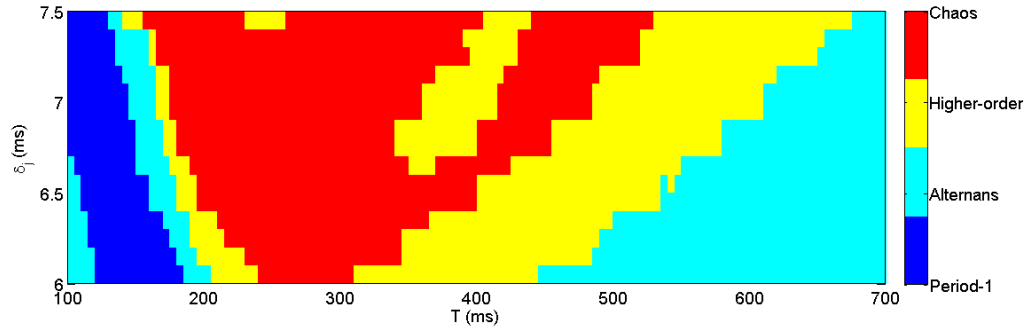

Figure 5.14: Approximate ranges of delays and periods over which period-1 (dark blue), alternans (cyan), higher-order (yellow) periodicities and unstable (red, chaotic) behavior occurred for large delays. Note that the physiologically normal SR release slope was used. For delays below 6 ms, no chaotic behavior occurred for any pacing period. For delays between 7.4 and 7.8 ms, there were 3 regions of instability that alternated with 4 stable regions, and at a delay of 8 ms, there were 4 regions of instability and 5 stable regions that switched back and forth.

These numerical simulations were done for 100 ms to ensure that transient dynamics were not interpreted as chaos when using our method outlined in Section 4.5 for each period between $T = 100$ ms and $T = 1000$ ms with a precision of 5 ms. We showed periods between $T = 100$ ms and $T = 700$ ms since chaos only appeared in this range of periods for the delays which began to produce chaos, and once higher-order periodicities transitioned into alternans, only alternans behavior occurred for pacing periods up to 1 s. Note that chaos did occur for longer periods, but only for significantly high delays (for example, chaos begins to occur with $T = 750$ ms only once $\delta_j \geq 8.8$ ms). With a normal SR release slope, chaotic behavior did not appear when the delay δ_j was below 6 ms. Once chaotic behavior began, the system maintained stability for very short or very long pacing periods. As the value of δ_j was increased, the regions became very complex. In the transition between 6.5 and 6.6 ms (seen in Figure 5.14), an additional chaotic and higher-order region appear, maintaining the alternating pattern from stability to instability and vice versa. A particularly interesting result of the appearance of additional stable and unstable regions is that for a fixed period, increasing the delay could cause the system to lose stability, regain stability as the delay continues to increase, and then lose stability again. This pattern could alternate several more times as the behavior of the system becomes more complex as the delay is increased further. A long-term prediction would be that for some large delay, only unstable behavior would occur and there would not exist any pacing periods for which stable, periodic behavior could happen. Also note that in our simulations, chaotic behavior did not occur for any pacing periods when the delay δ_j was below 3 ms.

Chapter 6

Discussion

6.1 Interpretations of Relaxation Time Constant τ_a and Delay δ_j

Two physical interpretations of the τ_a relaxation constant exist and are consistent with model results. τ_a could correspond to the diffusional delay from the NSR to JSR compartments suggested in Ref. [49], or it could be the refractoriness of RyR channels after calcium release from the SR as posed by Mahajan et al. [38] The relaxation time constant was ranged from 1 to 100 ms in Ref. [49], and Mahajan et al. solely used a time constant of 100 ms [38]. In experiments by Brochet et al., it was found that refilling of JSR compartments (called calcium blinks) had a time constant of 29 ms, while the combination of refilling JSR compartments plus the time for RyR channels to recover gave a time constant of 194 ms [7]. Mahajan et al. advocate that the latter of these interpretations is more likely, since they found that a combination of steep dependence of SR release on SR calcium content and a time delay in RyR recovery was necessary to produce alternans behavior [38]. Situations where the delay δ_j is very high could correspond to myocardial infarction, which has been suggested to be marked by a depression of RyR activity as suggested by Diaz et al. [15]

Our implementation of the calcium cycling model from Ref. [49] replaced Equation 4.7 and its associated relaxation time constant with our delay-differential formulation Equation 4.8, with constant delay δ_j. Alternans occurred for as small of a delay as 2.1 ms, and chaotic behavior appear for delays greater than or equal to 6 ms. Note that time constants and the delay are not directly analogous, although we believe that there may be a possible connection between the two. A larger time constant τ_a resulted in a larger release of calcium from the SR, as shown in Figure 4.1. A larger delay in our model corresponded to larger calcium peaks, and drove instabilities in the calcium dynamics. We also observed that for sufficiently small values of the delay, the right-hand side of Equation 4.8 is approximately equal to a time derivative in c'_j. Thus, for small values of δ_j, we would see nearly identical swings in c_j as in c'_j. This makes sense because a small delay would correspond to a very short diffusion time, meaning once calcium is pumped back into the NSR via the uptake current, the SR and JSR calcium concentrations experience the same increase in calcium at approximately the same time.

6.2 Model Limitations

There were situations where the delay was producing unrealistic behavior. Some peaks in myoplasmic calcium were greater than 10 μM, whereas values seen in experiments ranged from .1 μM to 3 μM [11]. This may be due to the possibility of a negative JSR calcium concentration. Also note that in Ref. [49], Shiferaw et al. state that the model they present (Equations 4.3 - 4.7) does not mathematically forbid unphysiological draining of the sarcoplasmic reticulum and that physiological parameters were adjusted to line up as closely as possible to experimental results, and to ensure that the SR calcium concentration was always positive. Given that some of our simulations did show unphysiological draining of the SR, the solution may be to phenomenologically determine parameter values after implementing a delay-differential equation into the model. Delay-differential equations are well-known to overshoot steady-state values as shown in Figure 4.2, and produce potentially unrealistic behavior. For example, common applications of DDEs are in the area of population dynamics. Many of these models have a population cap that is usually related to available resources and average lifetime, and in ODE-type models, this population cap generally is not breachable. Models that utilize DDEs, though, are sometimes able to

breach the population cap due to a delay. In the case of population dynamics, it is not reasonable to assume that members of a population will instantly die off if resources become scarce. Some DDE models account for this and make starvation a non-instantaneous event driven by the value of the delay associated with it. This delay makes it possible, given that the growth rate is high enough, for the population to breach its population cap, a phenomenon normally unseen in ODE models, although possible in difference equations. Is it possible that a similar thing is occurring in our ODE-DDE system when the value of c_j' drops below zero. We also computed numerical simulations with restricting the value of c_j' to be non-negative, the results of which are shown in Figure 6.1.

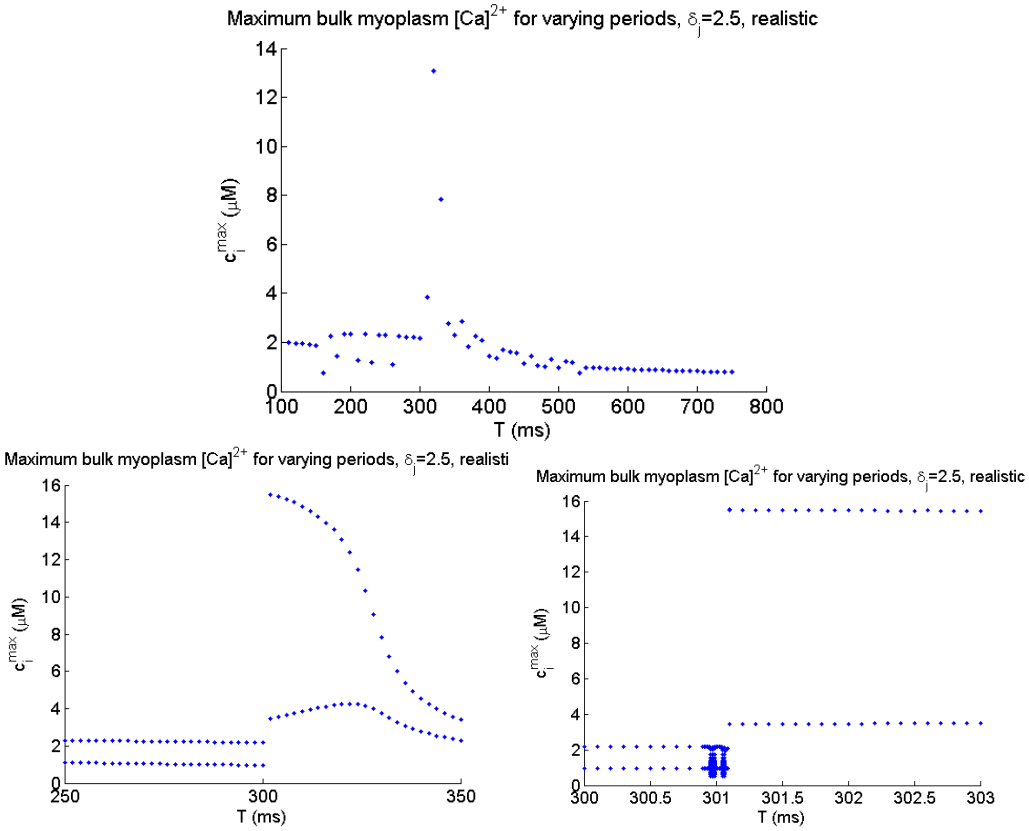

Figure 6.1: Bifurcation diagram of c_i^{max} versus period, restricting c_j' to non-negative values. Bottom graphs are finer simulations around the period where the peak values jump sharply. Alternans behavior is persistent for a wide range of periods (150 ms to 540 ms). Simulations around $T = 301$ ms did not appear to be chaotic in nature, but rather did not achieve steady-state values in a computationally feasible amount of time.

We saw in our models that when the JSR calcium concentration was held above zero, peak myoplasmic calcium values increased significantly (even beyond reasonable concentrations). The jump in concentration seen in Figure 6.1, though, is not aligned with when the JSR concentration would dip below zero. For this particular delay, negative values of c_j' were observed starting at a period of 310 ms. At a period of 301 ms, all values are positive and are physiologically reasonable. In Figure 6.2, we compare the time courses of myoplasmic and JSR calcium when the JSR concentration restricted to non-negative values to normal, unrestricted simulations where the JSR concentration is allowed to be negative.

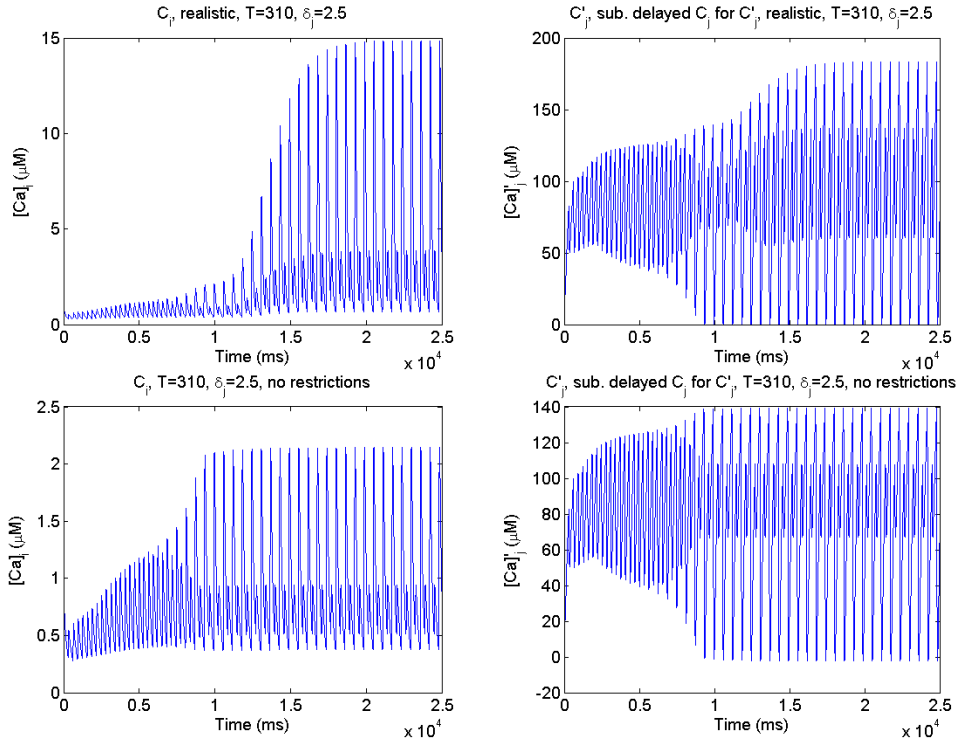

Figure 6.2: Top graphs: Bulk myoplasmic calcium concentration and JSR calcium concentration, for a pacing period of 310 ms and delay of 2.5 ms. JSR concentration is restricted to non-negative values, and this causes the myoplasmic concentration to increase up to 15 μM. Bottom graphs: Same simulation with identical period and delay, but without restricting the value of c'_j. JSR concentration reaches a minimum at about -2 μM, which is physically impossible. Despite this, the myoplasmic calcium concentration stays well within reasonable values.

Even though unrealistic values of c'_j were observed in simulations, myoplasmic concentrations were within reasonable limits for many solutions (see Figure 5.5). Shannon et al. found in their experiments that fractional release of calcium from the SR could be above 100%. The explanation they gave was that once the concentration of calcium in recruited JSR compartments was low enough, the overall SR calcium concentration falls below the average JSR concentration, and thus calcium diffuses along the gradient back into the SR, and then into currently emptying JSR compartments, resulting in a greater release of calcium from the SR. Meanwhlie, the SR is continually pumping calcium via the

uptake current, which could again be released during the same CICR event. This could be a possible explanation for the cases where c_j' becomes negative. Negative JSR calcium concentrations may also be alleviated if the total amount of calcium within the system is not held constant.

6.3 Comparison of ODE and DDE Models

We compared our results of implementing a delay-differential equation into the system of equations (Equations 4.3 - 4.7) from Ref. [49], by replacing Equation 4.7 with a first-order linear DDE (Equation 4.8). We were able to replicate alternans and chaotic behavior observed in Ref. [49], although the amplitude of alternans and magnitude of calcium peaks were sometimes larger than observed in simulations in Ref. [49]. We found that our results qualitatively validated our DDE implementation (see Figures 5.1 - 5.3, 5.5). A significant result of our research conducted was that the calcium cycling system was able to exhibit chaotic behavior without a steep SR release slope. A steep SR release slope has been cited as a crucial factor in producing dynamical instabilities in the intracellular calcium cycling system [4, 18, 38, 44, 49, 51]. In our DDE model, the delay implemented played a major role in determining the behavior of the system. We observed that chaos did not occur for any pacing period when $\delta_j < 6$ ms when using a physiologically normal SR release slope (11.3 $\mu M/s$ in Ref. [49]). We analyzed the behaviors of the calcium cycling system with a steep SR release slope as well (43.3 $\mu M/s$ in Ref. [49]), and saw that there were no qualitative changes, but simply that similar complex dynamics occurred at lower values of δ_j than compared to model simulations involving a physiologically normal SR release slope.

Chapter 7

Conclusion

To the best of our knowledge, this is the first application of delay-differential equations to cardiac modeling at the cellular level and in modeling calcium cycling in cardiac myocytes. In Chapter 1, we described the calcium cycling process within cardiac myocytes in detail, emphasizing phenomena like calcium-induced calcium release (CICR), transmembrane currents such as L-type calcium channels and exchanging currents (Na^{+}-Ca^{2+} exchanger). We also recounted the physiological processes involving the sarcoplasmic reticulum (SR), including calcium release via ryanodine receptor (RyR) channels, and uptake pumps regulated by sarcoendoplasmic reticulum calcium ATP-ase (SERCA). In addition, we briefly showed some physiological differences between the intracellular structures of ventricular and Purkinje cells. Cardiac alternans induced by instabilities in calcium or voltage (or both) has been an extensive area of research in cardiac electrophysiology. Our discussion of alternans has been thorough, describing and depicting possible mechanisms and triggers of irregular behavior in cardiac cells and at the level of tissue. Among the revelant behaviors are electromechanically concordant and discordant alternans, quasiperiodicity, and chaos (which has been hypothesized to describe ventricular fibrillation). We gave a short introduction to delay-differential equations (DDEs) and mentioned several applications common to the biological and physical sciences. We also found an application of DDEs to cardiac modeling in the context of studying alternans in a ring of excitable tissue.

After the background, we discussed the calcium cycling model to be used and proposed a DDE to replace the ODE describing diffusional flow between the network sarcoplasmic reticulum (NSR) and junctional sarcoplasmic reticulum (JSR). In replacing this equation, we implemented a delay δ_j in place of the time constant used in the original ODE (τ_a). There are different possible interpretations of the time constant τ_a and the delay we used δ_j, which we discussed in detail. We also described the chosen numerical method for solving the ODE-DDE system and outlined the necessary precautions and limitations that were required when solving a DDE numerically. A key quantitative measure in describing the intracellular calcium dynamics is the peak myoplasmic calcium concentration. We developed a simple and efficient way to calculate this, including an algorithm for determining periodicity, when patterns did appear in the calcium peaks.

Finally, we presented our results, and showed how the dynamical behavior of the ODE-DDE system was crucially dependent on the value of the delay implemented (δ_j). Alternans and chaotic behavior were exhibited, as well as the instance of higher-order periodicities. The progressions from periodic to aperiodic behavior were similar to those observed by Qu et al. and Hastings et al. [28, 44] We also illustrated the effect of steepening the SR release slope and established approximate boundaries for stable and unstable behavior seen in our dynamical system.

There are several opportunities for future research in applying delay-differential equations to cardiac modeling. Continuing the preliminary work here, the incorporation of our DDE into a full myocyte model could provide new insights into the degree to which delays affect the action potential and influence the coupling between calcium and voltage. We implemented a delay to account for the finite time it takes calcium to diffuse through the NSR into JSR compartments. There are several other instances in the intracellular calcium cycling model presented by Shiferaw et al. [49] where the diffusion of calcium between intracellular spaces is governed by a relaxation ordinary differential equation and could instead be represented by simple DDEs. Another possible utilization of DDEs in cardiac modeling is to describe the gating kinetics of ion channels. In this application, the delay could represent the time necessary for channel proteins to change conformationally in the process of opening and closing the ionic channel. Action potential models assume this process to be instantaneous. The implementation of a variable delay could be considered by taking $\delta_j = \delta_j(t, V, c_i, I_r, etc.)$, where the delay is a function of membrane potential,

intracellular calcium, the release current, etc. A variable delay could give new insight into modeling calcium restitution or the recovery of ryanodine receptors, as mentioned in Section 4.3.

In our discussion, we confronted some inconsistencies in our model with other calcium cycling models and experiments. Understanding the connections between relaxation ODEs and linear first-order DDEs should provide insight into how the non-instantaneous events with the system affect its dynamical behavior. Relaxation ODEs are common in mathematical models so deriving delayed equations could give physical processes new and intriguing meanings. Other approaches, including those that start from the ground up with delay-differential equations or analogies between cardiac systems and other biological systems, could prove useful in revealing more about how the cardiovascular system mechanistically works. DDEs are abundantly used to model population dynamics, and analogies between cardiac tissue and predator-prey systems have been made [41]. This preliminary analysis of using DDEs in modeling calcium cycling has shown that DDEs can be useful in modeling complex dynamical behavior and promises to be an expanding area of research in mathematical modeling.

Bibliography

[1] Murray E. Alexander, Seyed M. Moghadas, Gergely Röst, Jianhong Wu, et al., *A Delay Differential Model for Pandemic Influenza with Antiviral Treatment*, Bulletin of Mathematical Biology **70** (2007), no. 2, 382–397.

[2] J Scott Allison, Hao Qin, Derek J Dosdall, Jian Huang, Jonathan C Newton, James D Allred, et al., *The Transmural Activation Sequence in Porcine and Canine Left Ventricle is Markedly Different During Long-Duration Ventricular Fibrillation*, Journal Of Cardiovascular Electrophysiology **18** (2007), no. 12, 1306–1312.

[3] G. W. Beeler and H. Reuter, *Reconstruction of the Action Potential of Ventricular Myocardial Fibres*, Journal of Physiology **268** (1977), no. 1, 177–210.

[4] Harold Bien, Lihong Yin, and Emilia Entcheva, *Calcium Instabilities in Mammalian Cardiomyocyte Networks*, Biophysical Journal **90** (2006), no. 7, 2628–2640.

[5] Lothar A Blatter, Jens Kockskamper, Katherine A Sheehan, Aleksey V Zima, Jorg Huser, and Stephen L Lipsius, *Local Calcium Gradients During Excitation-Contraction Coupling and Alternans in Atrial Myocytes*, Journal of Physiology **546** (2003), no. Pt 1, 19–31.

[6] Gennadii A. Bocharov and Fathalla A. Rihan, *Numerical Modelling in Biosciences Using Delay Differential Equations*, Journal of Computational and Applied Mathematics **125** (2000), no. 12, 183–199.

[7] Didier X. P. Brochet, Dongmei Yang, Alessandro Di Maio, W. Jonathan Lederer, Clara Franzini-Armstrong, and Heping Cheng, *Ca^{2+} Blinks: Rapid Nanoscopic Store*

Calcium Signaling, Proceedings of the National Academy of Sciences **102** (2005), no. 8, 3099–3104.

[8] S. Cavalcanti and E. Belardinelli, *Modeling of Cardiovascular Variability Using a Differential Delay Equation*, IEEE Transactions on Biomedical Engineering **43** (1996), no. 10, 982–989.

[9] Shanshan Chen, Junping Shi, and Junjie Wei, *Time Delay-Induced Instabilities and Hopf Bifurcations in General Reaction-Diffusion Systems*, Journal of Nonlinear Science **23** (2012), no. 1, 1–38.

[10] E. M. Cherry and F. H. Fenton, *Visualization of Spiral and Scroll Waves in Simulated and Experimental Cardiac Tissue*, New Journal of Physics **10** (2008), no. 12, 125016.

[11] E. Chudin, J. Goldhaber, A. Garfinkel, J. Weiss, and B. Kogan, *Intracellular Ca^{2+} Dynamics and the Stability of Ventricular Tachycardia*, Biophysical Journal **77** (1999), no. 6, 2930–2941.

[12] Colleen E. Clancy and Yoram Rudy, *Linking a Genetic Defect to its Cellular Phenotype in a Cardiac Arrhythmia*, Nature **400** (1999), no. 6744, 566–569.

[13] Marc Courtemanche, Leon Glass, and James P. Keener, *Instabilities of a Propagating Pulse in a Ring of Excitable Media*, Physical Review Letters **70** (1993), no. 14, 2182–2185.

[14] Marc Courtemanche, James P. Keener, and Leon Glass, *A Delay Equation Representation of Pulse Circulation on a Ring in Excitable Media*, SIAM Journal on Applied Mathematics **56** (1996), no. 1, 24.

[15] M. E. Diaz, D. A. Eisner, and S. C. ONeill, *Depressed Ryanodine Receptor Activity Increases Variability and Duration of the Systolic Ca^{2+} Transient in Rat Ventricular Myocytes*, Circulation Research **91** (2002), no. 7, 585–593.

[16] Mary E. Diaz, Stephen C. ONeill, and David A. Eisner, *Sarcoplasmic Reticulum Calcium Content Fluctuation Is the Key to Cardiac Alternans*, Circulation Research **94** (2004), no. 5, 650–656.

[17] D. DiFrancesco and D. Noble, *A Model of Cardiac Electrical Activity Incorporating Ionic Pumps and Concentration Changes*, Philosophical Transactions of the Royal Society of London, Biological Sciences **307** (1985), no. 1133, 353–398.

[18] D. A. Eisner, H. S. Choi, M. E. Daz, S. C. ONeill, and A. W. Trafford, *Integrative Analysis of Calcium Cycling in Cardiac Muscle*, Circulation Research **87** (2000), no. 12, 1087–1094.

[19] Teresa Faria, *Stability and Bifurcation for a Delayed PredatorPrey Model and the Effect of Diffusion*, Journal of Mathematical Analysis and Applications **254** (2001), no. 2, 433–463.

[20] Jeffrey J. Fox, Jennifer L. McHarg, and Robert F. Gilmour, *Ionic Mechanism of Electrical Alternans*, American Journal of Physiology **282** (2002), no. 2, H516–H530.

[21] Alan Garfinkel, Young-Hoon Kim, Olga Voroshilovsky, Zhilin Qu, Jong R. Kil, Moon-Hyoung Lee, et al., *Preventing Ventricular Fibrillation by Flattening Cardiac Restitution*, Proceedings of the National Academy of Sciences **97** (2000), no. 11, 6061–6066.

[22] Alessio Gizzi, Elizabeth M. Cherry, Robert F. Gilmour, Stefan Luther, Simonetta Filippi, and Flavio H. Fenton, *Effects of Pacing Site and Stimulation History on Alternans Dynamics and the Development of Complex Spatiotemporal Patterns in Cardiac Tissue*, Frontiers in Physiology **4** (2013), 1–20.

[23] Alan S. Go, Dariush Mozaffarian, Vronique L. Roger, Emelia J. Benjamin, Jarett D. Berry, William B. Borden, et al., *Heart Disease and Stroke Statistics 2013 Update: A Report from the American Heart Association*, Circulation **127** (2013), no. 1, e6–e245.

[24] Joshua I. Goldhaber, Lai-Hua Xie, Tan Duong, Christi Motter, Kien Khuu, and James N. Weiss, *Action Potential Duration Restitution and Alternans in Rabbit Ventricular Myocytes: The Key Role of Intracellular Calcium Cycling*, Circulation Research **96** (2005), no. 4, 459–466.

[25] Georg A. Gottwald, *Bifurcation Analysis of a Normal Form for Excitable Media: Are Stable Dynamical Alternans on a Ring Possible?*, Chaos **18** (2008), no. 1, 013129.

[26] Georg A. Gottwald and Lorenz Kramer, *A Normal Form for Excitable Media*, Chaos **16** (2006), no. 1, 013122.

[27] S M Harrison and M R Boyett, *The Role of the Na^+-Ca^{2+} Exchanger in the Rate-Dependent Increase in Contraction in Guinea-Pig Ventricular Myocytes*, J Physiol **482** (1995), no. Pt 3, 555–566.

[28] Harold M. Hastings, Flavio H. Fenton, Steven J. Evans, Omer Hotomaroglu, Jagannathan Geetha, Ken Gittelson, et al., *Alternans and the Onset of Ventricular Fibrillation*, Physical Review Letters **62** (2000), no. 3, 4043–4048.

[29] A. L. Hodgkin and A. F. Huxley, *A Quantitative Description of Membrane Current and its Application to Conduction and Excitation in Nerve*, Journal of Physiology **117** (1952), no. 4, 500–544.

[30] Wenzhang Huang, *Global Dynamics for a Reaction-Diffusion Equation with Time Delay*, Journal of Differential Equations **143** (1998), no. 2, 293–326.

[31] Thomas J. Hund and Yoram Rudy, *Rate Dependence and Regulation of Action Potential and Calcium Transient in a Canine Cardiac Ventricular Cell Model*, Circulation **110** (2004), no. 20, 3168–3174.

[32] Alain Karma, *Spiral Breakup in Model Equations of Action Potential Propagation in Cardiac Tissue*, Physical Review Letters **71** (1993), no. 7, 1103–1106.

[33] Karma, Alain, *Electrical Alternans and Spiral Wave Breakup in Cardiac Tissue*, Chaos **4** (1994), no. 3, 461.

[34] Kenneth R. Laurita, Rodolphe Katra, Barbara Wible, Xiaoping Wan, and Michael H. Koo, *Transmural Heterogeneity of Calcium Handling in Canine*, Circulation Research **92** (2003), no. 6, 668–675.

[35] Pan Li and Yoram Rudy, *A Model of Canine Purkinje Cell Electrophysiology and Ca^{2+} Cycling Rate Dependence, Triggered Activity, and Comparison to Ventricular Myocytes*, Circulation Research **109** (2011), no. 1, 71–79.

[36] C. Luo and Y. Rudy, *A Dynamic Model of the Cardiac Ventricular Action Potential. I. Simulations of Ionic Currents and Concentration Changes*, Circulation Research **74** (1994), no. 6, 1071–1096.

[37] C. H. Luo and Y. Rudy, *A Model of the Ventricular Cardiac Action Potential. Depolarization, Repolarization, and their Interaction.*, Circulation Research **68** (1991), no. 6, 1501–1526.

[38] Aman Mahajan, Yohannes Shiferaw, Daisuke Sato, Ali Baher, Riccardo Olcese, Lai-Hua Xie, Ming-Jim Yang, et al., *A Rabbit Ventricular Action Potential Model Replicating Cardiac Dynamics at Rapid Heart Rates*, Biophysical Journal **94** (2008), no. 2, 392–410.

[39] D. Noble, *A Modification of the Hodgkin–Huxley Equations Applicable to Purkinje Fibre Action and Pacemaker Potentials*, Journal of Physiology **160** (1962), no. 2, 317–352.

[40] J Nolasco and R Dahlen, *A Graphic Method for Study of Alternation in Cardiac Action Potentials*, Journal of Applied Physiology **25** (1968), no. 2, 191–196.

[41] Niels F. Otani, Alisa Mo, Sandeep Mannava, Flavio H. Fenton, Elizabeth M. Cherry, Stefan Luther, et al., *Characterization of Multiple Spiral Wave Dynamics as a Stochastic Predator-Prey System*, Physical Review Letters **78** (2008), no. 2, 021913.

[42] Joseph M. Pastore, Steven D. Girouard, Kenneth R. Laurita, Fadi G. Akar, and David S. Rosenbaum, *Mechanism Linking T-Wave Alternans to the Genesis of Cardiac Fibrillation*, Circulation **99** (1999), no. 10, 1385–1394.

[43] Etienne J. Pruvot, Rodolphe P. Katra, David S. Rosenbaum, and Kenneth R. Laurita, *Role of Calcium Cycling Versus Restitution in the Mechanism of Repolarization Alternans*, Circulation Research **94** (2004), no. 8, 1083–1090.

[44] Zhilin Qu, Yohannes Shiferaw, and James N. Weiss, *Nonlinear Dynamics of Cardiac Excitation-Contraction Coupling: An Iterated Map Study*, Physical Review Letters **75** (2007), no. 1, 011927–1–011927–13.

[45] Zhilin Qu, James N. Weiss, and Alan Garfinkel, *Spatiotemporal Chaos in a Simulated Ring of Cardiac Cells*, Physical Review Letters **78** (1997), no. 7, 1387–1390.

[46] Qu, Zhilin and Weiss, James N. and Garfinkel, Alan, *Cardiac Electrical Restitution Properties and Stability of Reentrant Spiral Waves: a Simulation Study*, American Journal of Physiology **276** (1999), no. 1, H269–H283.

[47] T R Shannon, K S Ginsburg, and D M Bers, *Potentiation of Fractional Sarcoplasmic Reticulum Calcium Release by Total and Free Intra-Sarcoplasmic Reticulum Calcium Concentration*, Biophysical Journal **78** (2000), no. 1, 334–343.

[48] Thomas R. Shannon, Fei Wang, Jos Puglisi, Christopher Weber, and Donald M. Bers, *A Mathematical Treatment of Integrated Ca Dynamics Within the Ventricular Myocyte*, Biophysical Journal **87** (2004), no. 5, 3351–3371.

[49] Y. Shiferaw, M.A. Watanabe, A. Garfinkel, J.N. Weiss, and A. Karma, *Model of Intracellular Calcium Cycling in Ventricular Myocytes*, Biophysical Journal **85** (2003), no. 6, 3666–3686.

[50] Yohannes Shiferaw and Alain Karma, *Turing Instability Mediated by Voltage and Calcium Diffusion in Paced Cardiac Cells*, Proceedings of the National Academy of Sciences **103** (2006), no. 15, 5670–5675.

[51] Yohannes Shiferaw, Daisuke Sato, and Alain Karma, *Coupled Dynamics of Voltage and Calcium in Paced Cardiac Cells*, Physical Review Letters **71** (2005), no. 2, 021903–1–021903–5.

[52] Mari Watanabe, Niels F. Otani, and Robert F. Gilmour, *Biphasic Restitution of Action Potential Duration and Complex Dynamics in Ventricular Myocardium*, Circulation Research **76** (1995), no. 5, 915–921.

[53] Mari A. Watanabe and Marcus L. Koller, *Mathematical Analysis of Dynamics of Cardiac Memory and Accommodation: Theory and Experiment*, American Journal of Physiology **282** (2002), no. 4, H1534–H1547.

[54] Yanni Xiao and Lansun Chen, *Modeling and Analysis of a Predator-Prey Model with Disease in the Prey*, Mathematical Biosciences **171** (2001), no. 1, 59–82.

[55] Jiang Xiao-Wei, Guan Zhi-Hong, Zhang Xian-He, Zhang Ding-Xue, and Liu Feng, *Stability and Neimark-Sacker Bifurcation Analysis of a Food-Limited Population Model with a Time Delay*, Chinese Physics Bulletin **22** (2013), no. 3, 030204.

[56] Ali R. Yehia and Dominique Jeandupeux, *Hysteresis and Bistability in the Direct Transition from 1:1 to 2:1 Rhythm in Periodically Driven Single Ventricular Cells*, Chaos **9** (1999), no. 4, 916.

Appendix A

Bifurcation Diagram Progressions

We include two progressions of calcium dynamics as the delay is increased, one with a physiologically normal SR release slope (11.3 $\mu M/s$, Figure A.1), and another progression with a steep SR release slope (43.3 $\mu M/s$, Figure A.2). As discussed in Sections 5.3 and 5.4, as the value of δ_j was increased, alternans and high-order periodicities accompanied transitions into and out of chaotic regions. At a delay of 3.3 ms, alternans behavior appeared in a straightforward manner. Then, at a value of 5.5 ms, alternans began to develop, but then stabilizes into period-1 behavior as the overall calcium peak magnitude increases from about 1.5 μM at the initiation of alternans, to slightly above 3 μM. At a delay of 7.1 ms, a similar stablization occurs, until alternans and then a period-4 solution appears. Before chaos occurs at $\delta_j = 7.9$, a period-3 solution was observed, and reached steady-state fast, as the corresponding return map shows. As the value of δ_j increased, the calcium dynamics transitioned out of chaos, and presented alternans that rapidly achieved steady-state. Eventually, at $\delta_j = 13$ ms, chaotic dynamics returned.

For a steep SR release slope there were multiple transitions into and out of chaos observed, and in general steady-state was achieved more quickly, as the accompanying return maps show in Figure A.2. Similar progressions into and out of chaos were observed for situations involving a steep SR release slope. These dynamics did occur at lower values of δ_j though, and the overall magnitude of calcium peaks observed was significantly higher than with a physiologically normal release slope.

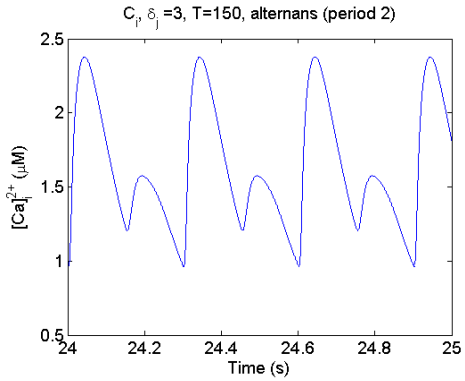
C_i, δ_j =3, T=150, alternans (period 2)
[Ca]_i^2+ (μM)
Time (s)

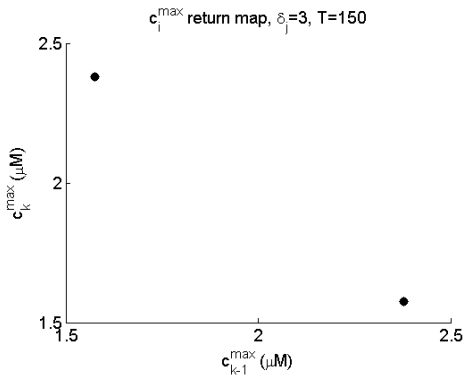
c_i^max return map, δ_j=3, T=150
c_k^max (μM)
c_k-1^max (μM)

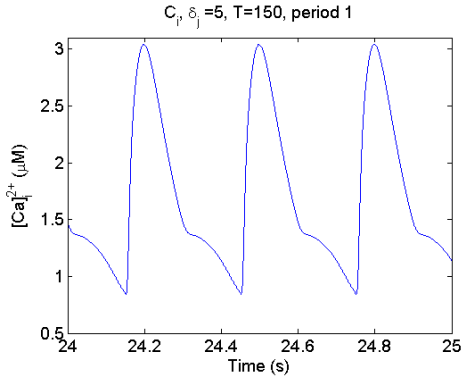
C_i, δ_j =5, T=150, period 1
[Ca]_i^2+ (μM)
Time (s)

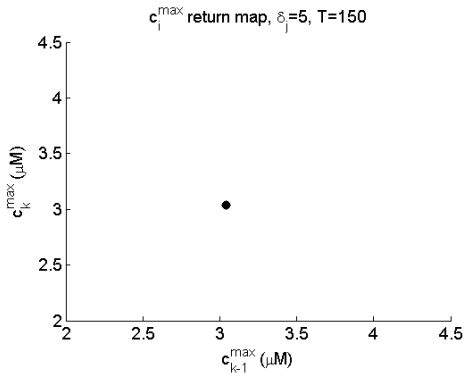
c_i^max return map, δ_j=5, T=150
c_k^max (μM)
c_k-1^max (μM)

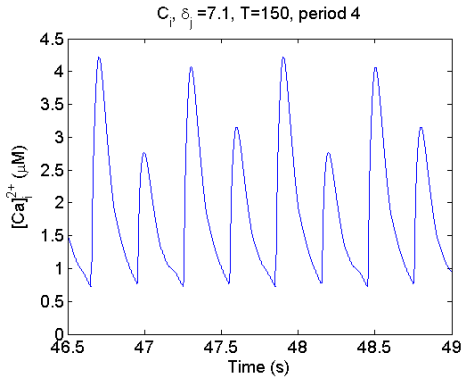
C_i, δ_j =7.1, T=150, period 4
[Ca]_i^2+ (μM)
Time (s)

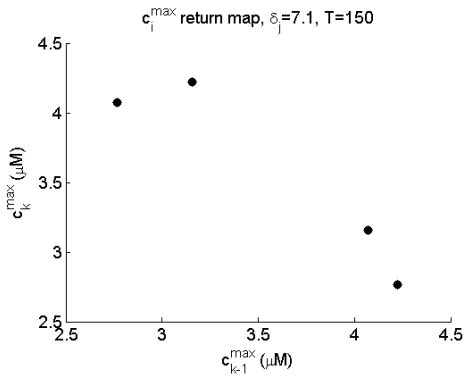
c_i^max return map, δ_j=7.1, T=150
c_k^max (μM)
c_k-1^max (μM)

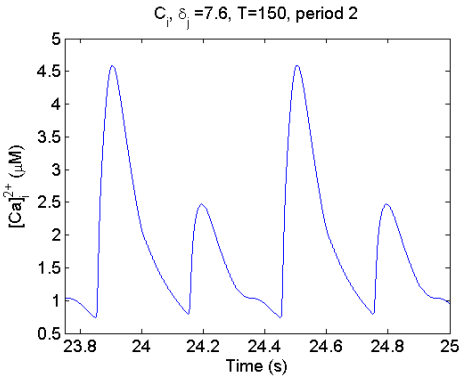
C_i, δ_j =7.6, T=150, period 2
[Ca]_i^2+ (μM)
Time (s)

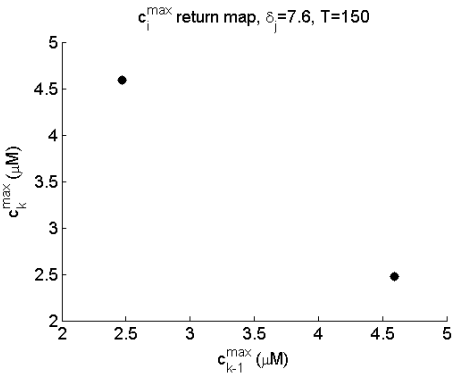
c_i^max return map, δ_j=7.6, T=150
c_k^max (μM)
c_k-1^max (μM)

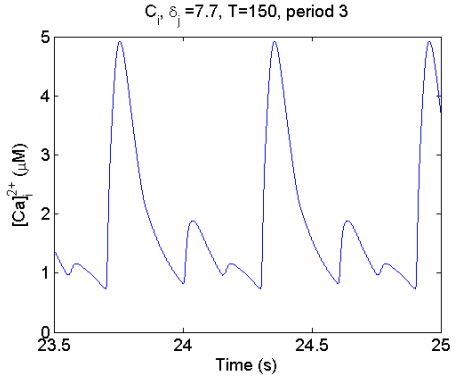
C_i, δ_j =7.7, T=150, period 3
[Ca]_i^2+ (μM)
Time (s)

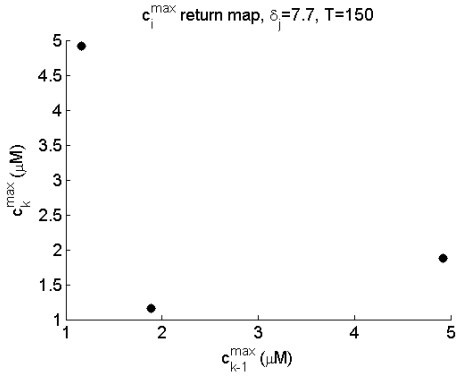
c_i^max return map, δ_j=7.7, T=150
c_k^max (μM)
c_k-1^max (μM)

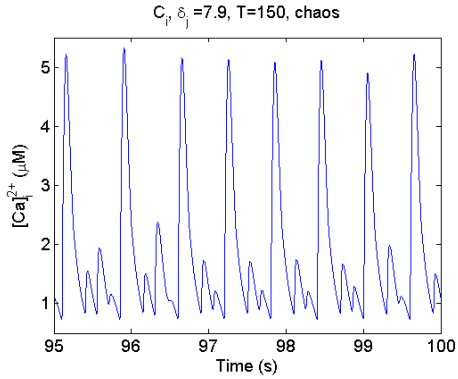
C_i, δ_j =7.9, T=150, chaos
[Ca]_i^2+ (μM)
Time (s)

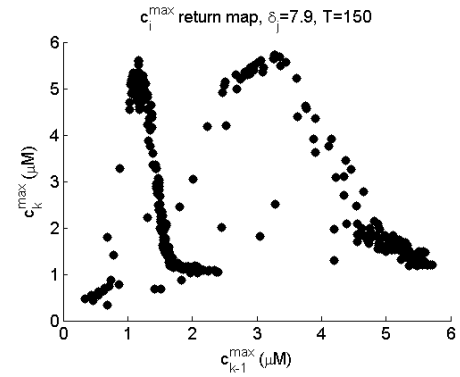
c_i^max return map, δ_j=7.9, T=150
c_k^max (μM)
c_k-1^max (μM)

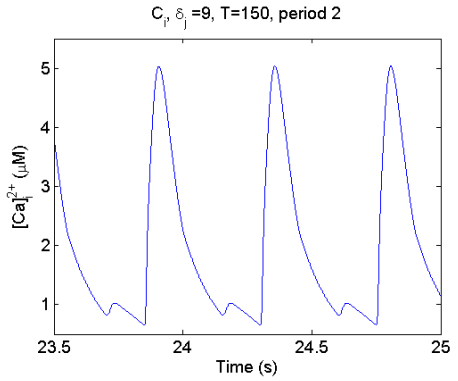
C_i, δ_j =9, T=150, period 2
[Ca]_i^2+ (μM)
Time (s)

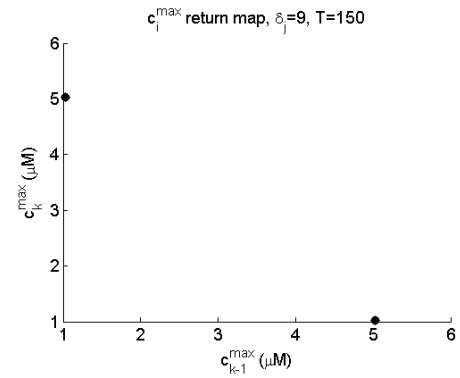
c_i^max return map, δ_j=9, T=150
c_k^max (μM)
c_k-1^max (μM)

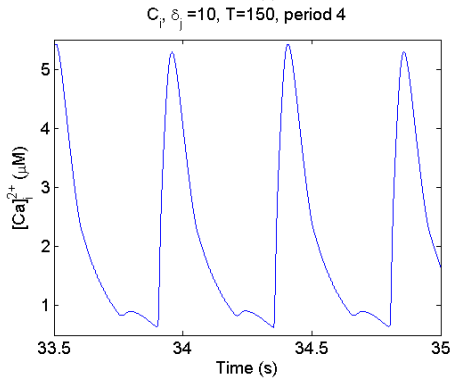
C_i, δ_j =10, T=150, period 4
[Ca]_i^2+ (μM)
Time (s)

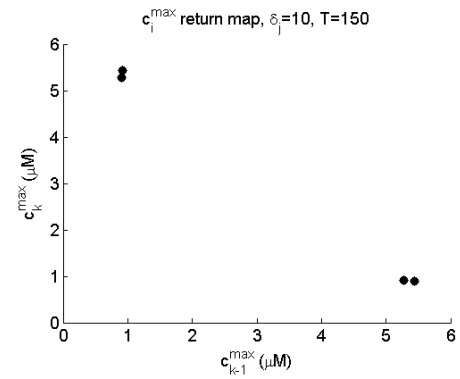
c_i^max return map, δ_j=10, T=150
c_k^max (μM)
c_k-1^max (μM)

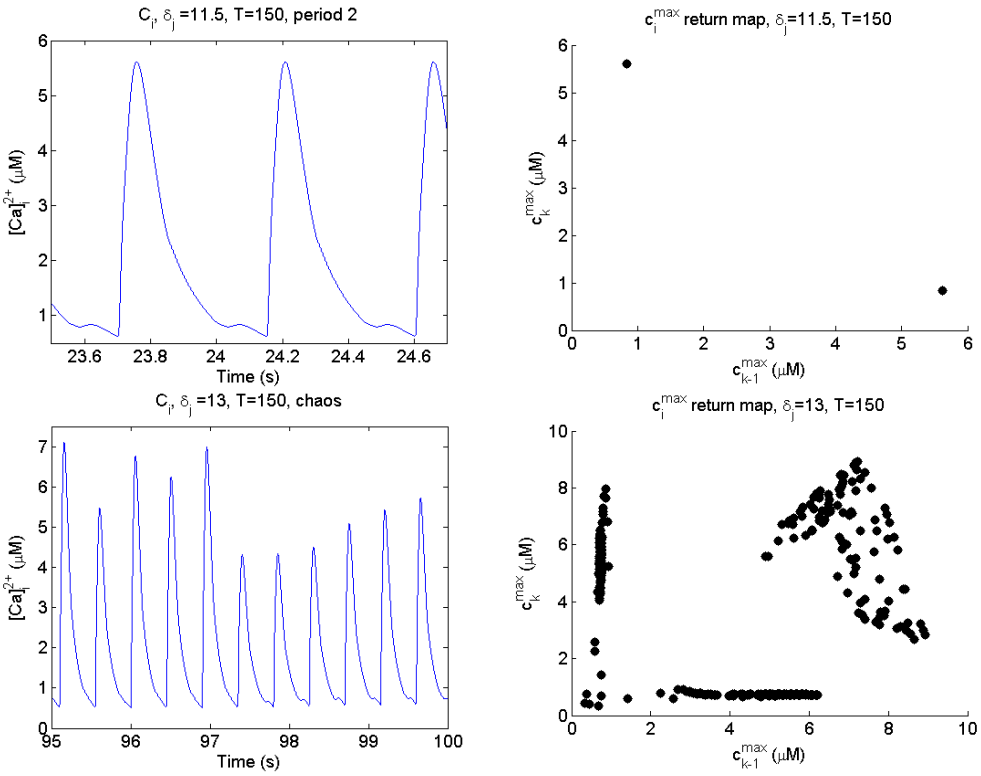

Figure A.1: Transitions between several different periodic and chaotic behaviors as δ_j is increased. The period was held constant at 150 ms, and the timescales differ depending on how quickly steady-state behavior was achieved. Return maps on the right relate consecutive myoplasmic calcium peaks. Red dots correspond to peaks that occur near the beginning of the simulation, whereas dark blue dots correspond to calcium peak values towards the end of the simulation time (100 s). Solutions that quickly resolved show mostly red and orange dots, and dark blue dots representing steady-state. Solutions that took longer to reach steady-state will show a wider range of colors from red to orange to yellow to green, and eventually to dark blue. Chaos observed showed no steady-state solutions in the return maps.

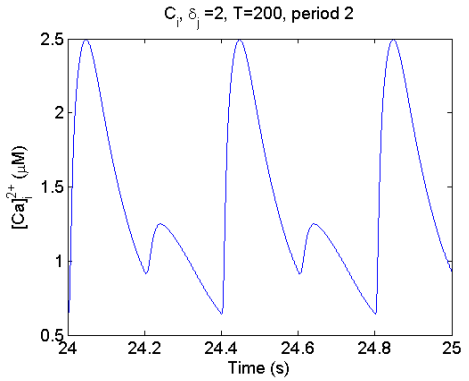
C_i, δ_j =2, T=200, period 2
[Ca]_i^2+ (μM)
Time (s)

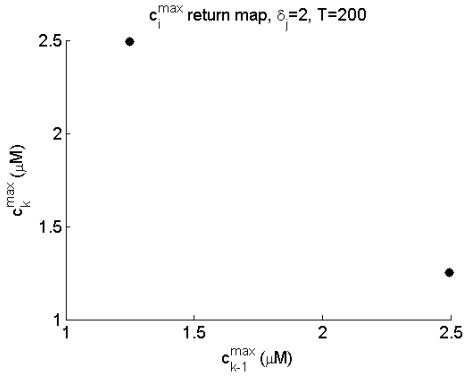
c_i^max return map, δ_j=2, T=200
c_k^max (μM)
c_k-1^max (μM)

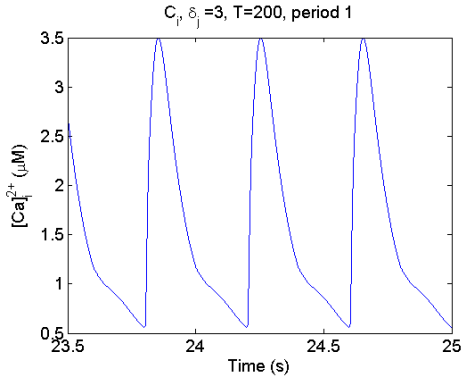
C_i, δ_j =3, T=200, period 1
[Ca]_i^2+ (μM)
Time (s)

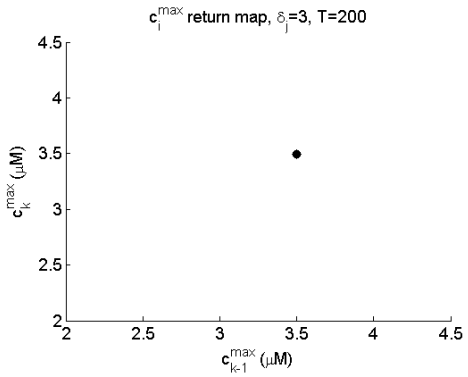
c_i^max return map, δ_j=3, T=200
c_k^max (μM)
c_k-1^max (μM)

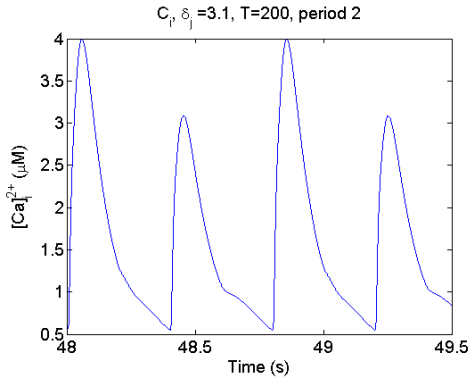
C_i, δ_j =3.1, T=200, period 2
[Ca]_i^2+ (μM)
Time (s)

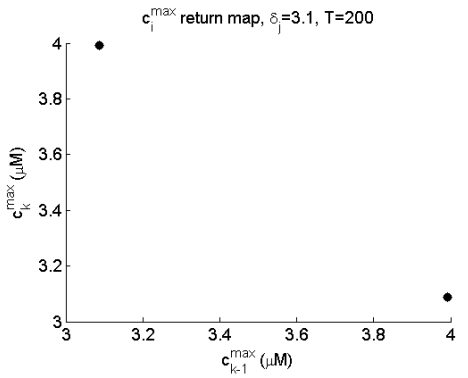
c_i^max return map, δ_j=3.1, T=200
c_k^max (μM)
c_k-1^max (μM)

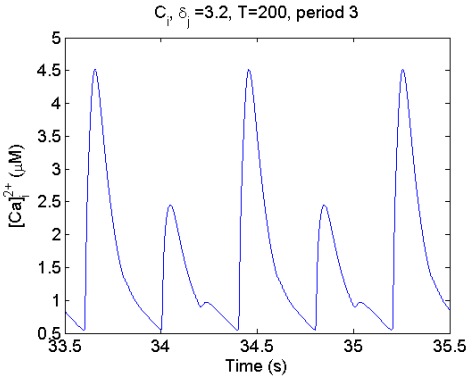
C_i, δ_j =3.2, T=200, period 3
[Ca]_i^2+ (μM)
Time (s)

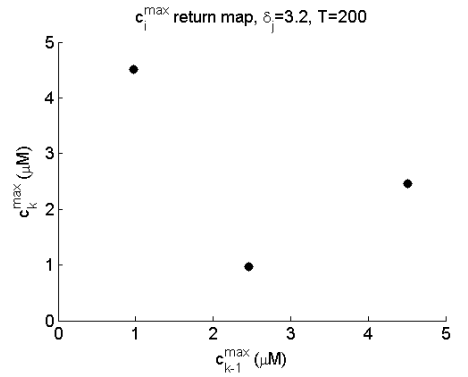
c_i^max return map, δ_j=3.2, T=200
c_k^max (μM)
c_k-1^max (μM)

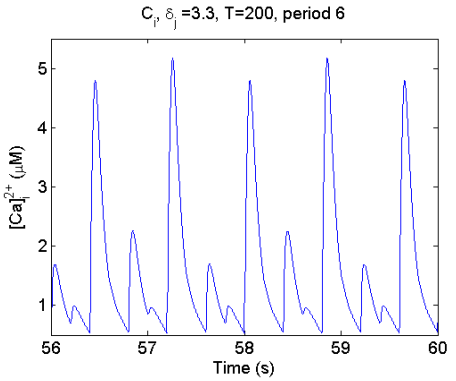
C_i, δ_j =3.3, T=200, period 6
[Ca]_i^2+ (μM)
Time (s)

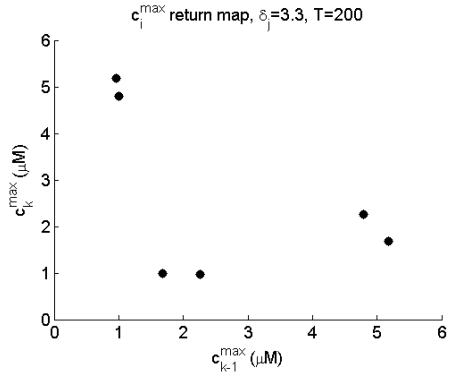
c_i^max return map, δ_j=3.3, T=200
c_k^max (μM)
c_k-1^max (μM)

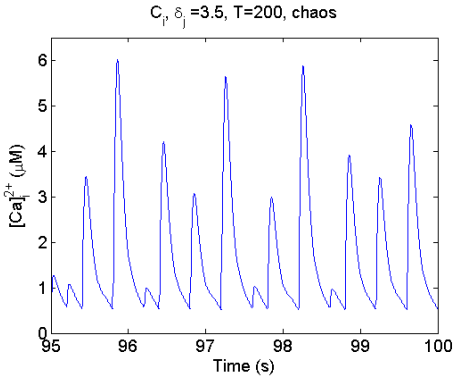
C_i, δ_j =3.5, T=200, chaos
[Ca]_i^2+ (μM)
Time (s)

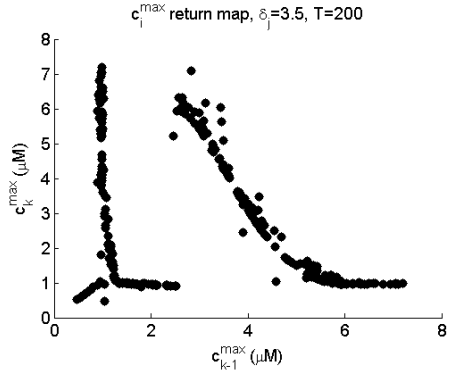
c_i^max return map, δ_j=3.5, T=200
c_k^max (μM)
c_k-1^max (μM)

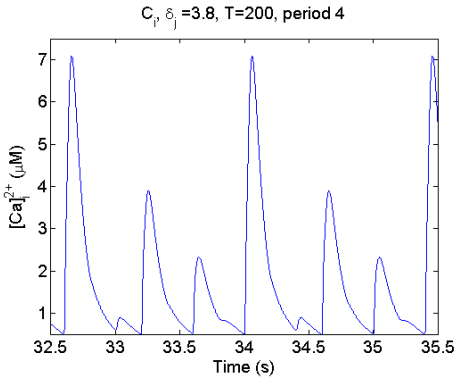
C_i, δ_j =3.8, T=200, period 4
[Ca]_i^2+ (μM)
Time (s)

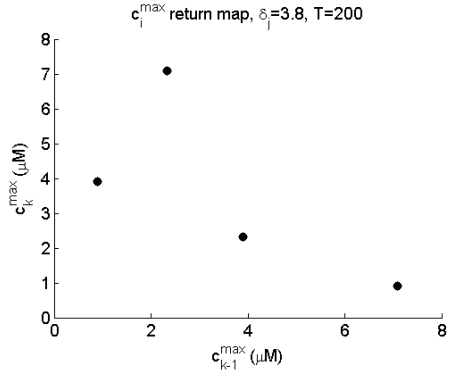
c_i^max return map, δ_j=3.8, T=200
c_k^max (μM)
c_k-1^max (μM)

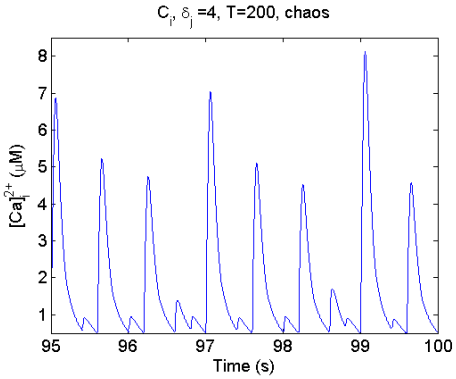
C_i, δ_j =4, T=200, chaos
[Ca]_i^2+ (μM)
Time (s)

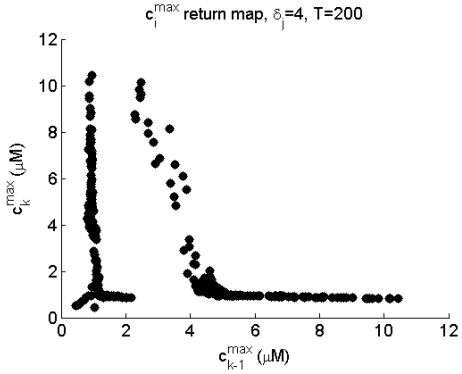
c_i^max return map, δ_j=4, T=200
c_k^max (μM)
c_k-1^max (μM)

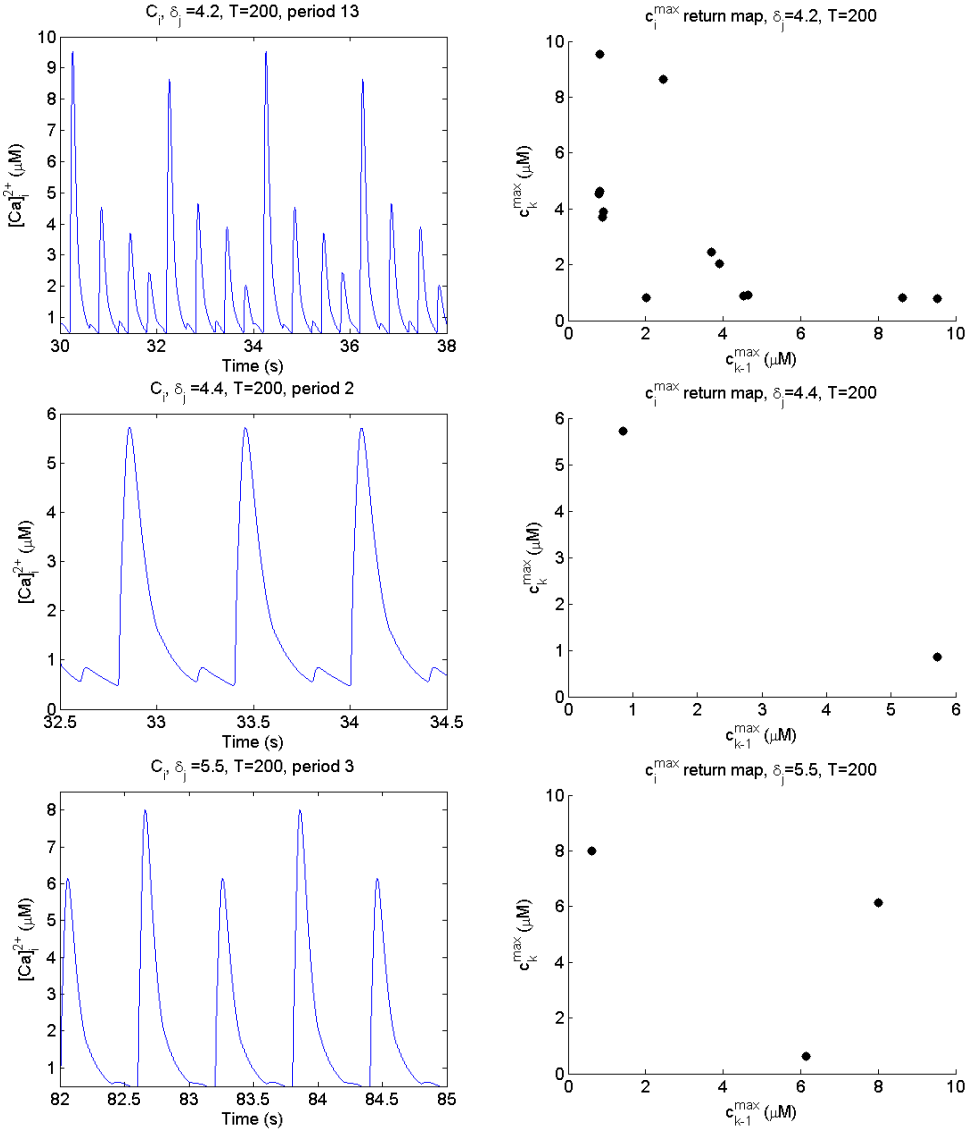
C_i, δ_j =4.2, T=200, period 13
[Ca]_i^2+ (μM)
Time (s)
c_i^max return map, δ_j=4.2, T=200
c_k^max (μM)
c_k-1^max (μM)
C_i, δ_j =4.4, T=200, period 2
[Ca]_i^2+ (μM)
Time (s)
c_i^max return map, δ_j=4.4, T=200
c_k^max (μM)
c_k-1^max (μM)
C_i, δ_j =5.5, T=200, period 3
[Ca]_i^2+ (μM)
Time (s)
c_i^max return map, δ_j=5.5, T=200
c_k^max (μM)
c_k-1^max (μM)

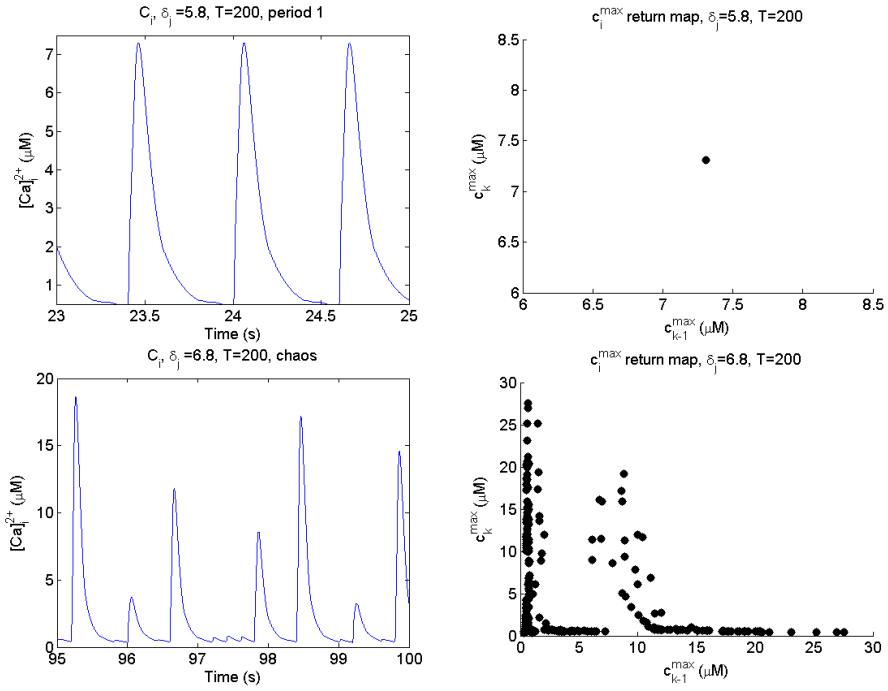

Figure A.2: Transitions between several different periodic and chaotic behaviors as the value of the delay δ_j was increased, using a steep SR release slope (43.3 $\mu M/s$). The period was held constant at 200 ms, and timescales differ depending on how quickly steady-state behavior was achieved. Return maps on the right relate consecutive myoplasmic calcium peaks. Red dots correspond to peaks that occur near the beginning of the simulation, whereas dark blue dots correspond to calcium peak values towards the end of the simulation time (100 s). Solutions that quickly resolved show mostly red and orange dots, and dark blue dots representing steady-state. Solutions that took longer to reach steady-state will show a wider range of colors from red to orange to yellow to green, and eventually to dark blue. Chaos observed showed no steady-state solutions in the return maps.